Thin–Walled Structures 192 (2023) 111207

Contents lists available at ScienceDirect

Thin-Walled Structures

journal homepage: www.elsevier.com/locate/tws

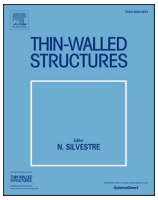

Full length article

Confinement-based direct design method for fibre reinforced polymer confined CFST short columns

M.F. Hassanein [a], Asmaa Y. Hamed [b], K.A. Cashell [c,*], Yong-Bo Shao [d]

[a] Department of Structural Engineering, Faculty of Engineering, Tanta University, Tanta, Egypt
[b] Construction and Building Department, The Higher Institute of Engineering and Technology Luxor, Egypt
[c] Department of Civil, Environmental and Geomatic Engineering - UCL – University College London, England, United Kingdom
[d] School of Civil Engineering and Geomatics, Southwest Petroleum University, Chengdu, Sichuan, 610500, China

ARTICLE INFO

Keywords:
Concrete filled steel tube
Circular CFST
Square CFST
CFRP
GFRP
Lateral confining stress
Design Resistance
Short column

ABSTRACT

The paper presents a detailed analysis of the behaviour of circular and square concrete filled steel tube (CFST) short columns strengthened externally with carbon or glass fibre reinforced polymer sheets (CFRP or GFRP, respectively). A thorough review of existing test information is presented and discussed, and the most salient parameters in terms of the overall strength are identified. There are a large number of influential and inter-related parameters which affect the load-carrying capacity, including the geometry, cross-sectional shape, type of steel, concrete strength, boundary and loading conditions, and type of FRP. It is shown that existing design approaches do not reliably predict the strength for the full range of possible parameters. Therefore, this paper proposes a new design model to calculate the axial compressive strength of FRP-confined concrete filled steel tubular (CFST) short columns with either a circular or square cross-section. The method accounts for the various complexities which affect the behaviour, yet presents a user-friendly, performance-based design expression. It is based on an evaluation of the lateral confining pressure provided by the both the FRP and the steel tube to the concrete core. This is employed in the confinement-based direct resistance calculations. The paper validates the approach by comparing its capacity predictions with a large database of experimental results and alternative design models available in the literature. The results show that the proposed model provides much accurate strength predictions with greater reliability for the full range of parameters examined, than existing methods.

1. Introduction

In recent years, there has been a significant increase in the use of concrete filled steel tubular (CFST) columns, largely owing to their efficiency and very high load-carrying capacity. There are a range of different varieties of CFST members with researchers generally focussing on the use of different materials, various cross-sectional arrangements such as concrete-filled double skin tubular (CFDST) members, and also CFST columns with additional materials such as fibre reinforced polymer (FRP) wrapped around the outside of the steel tube to improve the performance. The focus of the current paper is the latter, where FRP-confined CFST columns have been employed in structural applications such as bridges and buildings (see Fig. 1) due to their excellent strength-to-weight characteristics, high fatigue strength and excellent corrosion resistance [1–3].

FRP is a versatile composite material made up of a polymer matrix reinforced with fibres. There are a number of different types of FRP used in construction, and the most common forms are carbon fibre reinforced polymers (CFRP), glass fibre reinforced polymers (GFRP) and basalt fibre reinforced polymers (BFRP). Each variety of FRP has unique properties that make it suitable for different applications. The current paper is concerned with employing FRP to wrap around the outside of CFST columns, in order to increase the load-bearing capability by providing additional confining stress to the concrete core. As a result, these members offer excellent strength and stability compared with regular CFST columns, especially under extreme loading scenarios such as during earthquakes or high wind loads [4,5]. In addition, their dynamic response is improved under cyclic loading events like those encountered during an earthquake [6].

There are a large number of articles in the literature on FRP-confined circular or square CFST columns, including both experimental and

* Corresponding author.
E-mail address: k.cashell@ucl.ac.uk (K.A. Cashell).

https://doi.org/10.1016/j.tws.2023.111207
Received 2 May 2023; Received in revised form 4 August 2023; Accepted 18 September 2023
Available online 22 September 2023

Symbols

A_c	Cross-sectional area of the concrete
A_s	Cross-sectional area of the steel tube
A_f	Cross-sectional area of the FRP wrapping
A_{cs}	Total cross-sectional area of the CFST column case neglecting the area of the FRP
D	Outer diameter of the circular steel tube
D_c	Diameter of the infill concrete
E_c	Elastic modulus of the concrete
E_f	Elastic modulus of the CFRP or GFRP
E_s	Elastic modulus of the steel
E_{sc}	Elastic modulus of the composite section for CFRP-confined sections
f_{cu}	Cubic compressive strength of concrete
f_c	Compressive strength of the unconfined concrete
f_{ys}	Yield strength of the steel
f_{rp}	Lateral confining stress
f_{tf}	Tensile strength of the CFRP
L	Length of the stub column
n_f	Number of layers of CFRP or GFRP
t_s	Wall thickness of the steel tube
t_f	Wall thickness of one layer of CFRP or GFRP
P	Axial load
P_i	Design resistance (i varies depending on the source document)
$P_{u\text{-}Exp}$	Ultimate capacity of CFRP-confined CFT stub columns obtained from experimental results
r	Corner radius
ξ_s	Confinement index of the steel tube $\xi_s = \frac{A_s f_y}{A_c f_c}$
ξ_f	Confinement index of the CFRP or GFRP $\xi_f = \frac{A_f f_f}{A_c f_c}$
M	Average ratio of the measured-to-nominal material yield strengths
F	Average ratio of the measured-to-nominal dimensions of the cross-section
V_M	COV of M
V_F	COV of F
V_P.	COV of P
β	Reliability index
φ	Resistance factor
α	Sensitivity factor for the resistance
ε_f	Strain of CFRP
σ_{cf}	Stress of CFRP
σ_i	Equivalent stress of the steel
E_{st}	Strengthening modulus of steel
ζ	Strengthening coefficient of steel
D/t	Column Slenderness
σ_L	Axial compressive stress of the steel
σ_{hs}	Confining pressure around the concrete

numerical studies (e.g. [7–50]) The main parameters examined are the thickness and number of FRP layers [7-9,16], the FRP type (GFRP, CFRP or BFRP), the type of steel tube (normal-strength steel (NSS), high-strength steel (HSS) or stainless steel), the diameter to thickness ratio of the steel tubes [51,52], and the grade of concrete (normal--strength concrete (NSC), high strength concrete (HSC) and ultra-high strength concrete (UHSC)) [10–14]. Overall, a review of the available literature shows that the dominant failure modes of FRP-confined CFST columns are different than those of CFST columns in that the common failure mode for CFST columns, which is local buckling of the steel tube, is generally eliminated until the FRP layers fracture at the ultimate load level. Thus, the volume expansion of concrete is not as pronounced as in CFST columns.

Parvin and Jamwal [53] studied the influence of ply angle and ply crystalline structure coupled with the wrapping thickness on FRP-confined short columns using a nonlinear numerical simulation. The reliability of numerical methods with "angle-hoop-angle" and "hoop angle-hoop" ply configurations was evaluated, where "angle" and "hoop" denote wraps of 45° and 0° with respect to the circumferential direction, respectively. The results showed that the ply design has an effect on the axial stress and strain, and indicated that increasing the wrapping thickness improves the strength and ductility of the member. Other studies [32,34] showed that the best confinement occurs when the fibres are aligned with the direction of hoop stresses because (1) additional confinement due to the wrap enhances the compressive strength of the core, and (2) the presence of the FRP wrapping delays outward buckling of the steel tube, and consequent failure. Overall, most experimental tests on FRP-confined circular CFST columns indicated that the type and mechanical properties of the FRP are the main parameters affecting the ultimate strengths of the columns.

On other hand, wrapped CFST columns with a square cross-section are prone to earlier failure due to the concentration of stresses in the corner regions [15,36-38,40-44,51]. As a result of this, the failure mechanism of FRP-confined square CFST columns is more complex compared with circular columns. Overall, there have been fewer studies into the behaviour of FRP-confined square CFST columns compared with circular columns. The experimental and numerical study by Wei, et al. [38] indicated that increasing the corner radius of the square cross-section increases the ultimate strength of the column. Other studies [19,28,12] examined the effect of using different types of FRP material (i.e. carbon, glass or basalt FRP), which was shown to also be influential to the overall performance.

With regard to column resistance, different studies provided approaches for estimating the ultimate bearing capacity of FRP-confined circular and square CFST columns. Some (e.g. [45-49,9,54]) proposed estimating the ultimate axial load of circular CFST confined with CFRP based on the confinement stress of the FRP and the steel tube. Other approaches (e.g. [6,7,10-14,28,43,46]) considered two main enhancement factors: the steel confinement index and the FRP confinement index. All of the proposed models in the literature, with the exception of those given in [15,38,42,47], were examined and validated based on the authors own experimental test data rather than using independent data. Moreover, most of these design models focused on FRP-confined CFSTs with circular cross-sections, while very few models predicted the ultimate strength of FRP-confined CFST with a square cross-section. Additionally, the effect of different types of FRP such as CFRP and GFRP on the compressive resistance was investigated [8,13,32-35], and it was shown that the presence of all FRPs as the outside layer of the columns increases the axial capacity as well as the ductility.

Although it is clear that there has been good progress in developing the understanding of these elements, there are also some shortcomings in the design methods proposed. These are mainly related to the lack of a thorough reliability analysis for the various proposed design models and also, none of the previous investigations have examined their proposals over the full realistic steel tube slenderness range. In light of this, the main objective of this paper is to develop an explicit and direct method for designing circular and square CFST short columns confined with CFRP or GFRP. This is done by considering the confinement provided by the outer steel tube and the FRP. First, the experimental data of 324 circular and square CFST short columns confined with CFRP or GFRP were collected from the literature and are examined herein [7–44]. All of these columns were made using a carbon steel outer tube, wrapped on the outside with either CFRP or GFRP, and infilled with either normal (NSC), high strength (HSC) or ultra-high strength (UHSC) concrete with

a compressive strength of up to 120 MPa. Secondly, the collected data was used to evaluate 16 different design resistance models proposed in the literature [7,9-15,18,28,32,38-39,42-45]. As a result of this study, a new more accurate design model was developed and is described in this paper. This is a confinement-based direct design strength model based on a proposed confining stress (f_{rp}) which was determined from the experimental data.

2. Summary of the test data

Tables 1 and 2 summarise the available test data from the literature on FRP-confined circular and square CFST short columns, respectively. For all of the tests included in these tables, the specimens were loaded monotonically and concentrically under axial compression, and the FRP was wrapped transversely around the steel tube (i.e. ply angle=0). The tables provide the geometric and material properties of the steel tubes, FRP and unconfined concrete. For the FRP, the important properties include the thickness of one layer of FRP (t_f), number of layers (n_f), fibre type (CFRP or GFRP), tensile strength (f_{tf}) and elastic modulus (E_f). For the steel tubes, the properties presented include the effective length (L), diameter/depth (D) and thickness (t_s) as well as the yield strength (f_{ys}), whilst the compressive strength of the unconfined concrete (f_c) is also given.

The data from a total of 324 tests conducted in 38 different experi-

(a)

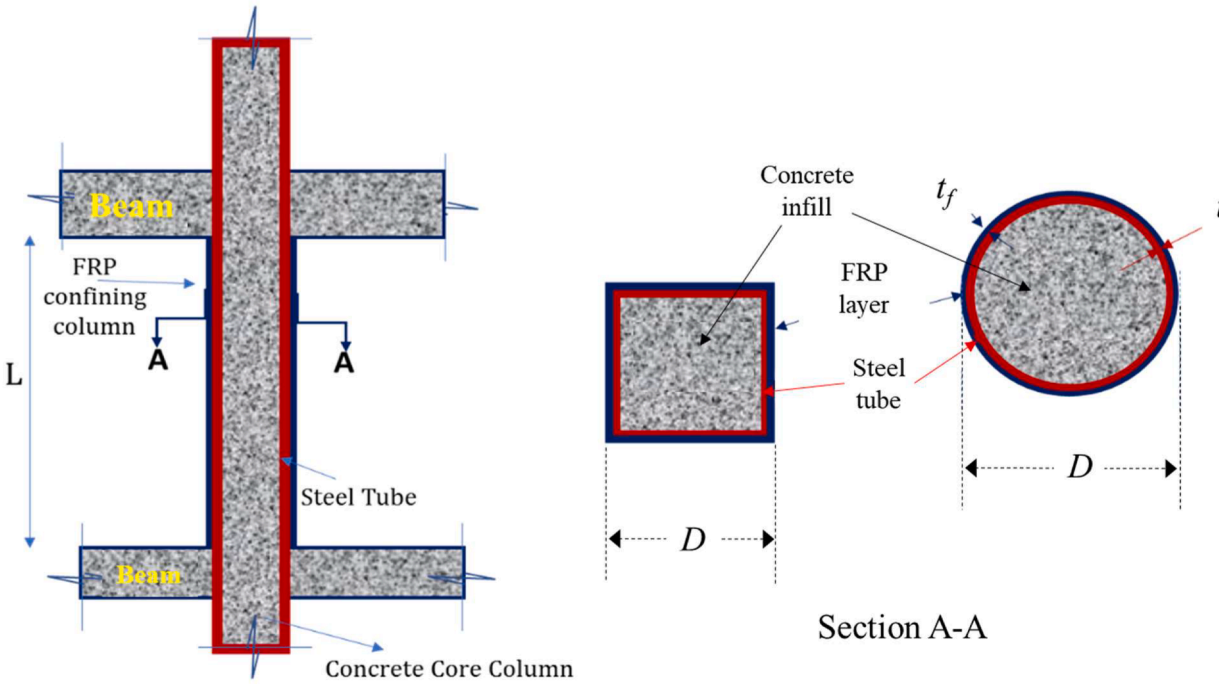

(b)

Fig. 1. CFRP-confined CFST columns including (a) photographic images of the circular columns in a bridge in Nanjing City, PR China [39] and (b) schematic views of both square and circular cross-sections.

Table 1
Geometric and material properties of tests on FRP-confined circular CFST short columns.

Ref.	No.	FRP Type	Geometric properties							Material Properties					$P_{u\text{-}Exp}$ (*kN*)
			L (mm)	D (mm)	t_s (mm)	D/t_s	L/D	t_f (*mm*)	n_f	*Steel* f_{ys} (MPa)	*FRP* f_{tf} (MPa)	E_f (*GPa*)	*Concrete* f_c (MPa)	
Wei et al. [7]	16	CFRP	400	133	3–7.5	17.7–44.3	3.01	0.11	1–2	248–365	4067.0	239	31.2–34.7	1179–2363
Liu and Lu [8]	7	CFRP	400	126–130	3–5	26–42	3.08–3.13	0.11	1–3	248	4067	239	37.36–51.43	1330–1658
	3	GFRP	400	128	4	32	3.13	0.169	1–3	248	2930	109	37.36	1355–1845
Park et al. [9]	7	CFRP	620	139.8	3.2–6.6	21.2–48.7	4.43	0.11	1–3	301–365	3500	200	30.61	1409–2275
Tao et al. [10]	4	CFRP	470–750	156–250	3	52–83.3	3	0.17	1–2	230	4212	255	46	1890–4780
Liu et al. [11]	16	CFRP	600–780	200–260	2	100–130	3	0.167	2–4	264	3400	235	48.7–57.88	2607–5374
Lu et al. [12]	7	CFRP	400	126–130	3–5	26–42	3.08–3.17	0.111	1–3	242–248	3550	250	37.36–51.43	1300–1658
	3	GFRP	400	128	4	32	3.13	0.169	1–3	248	2930	109	35.92	1356–1845
Che et al. [13]	10	CFRP	381–408	127–136	1.5–6	22.7–84.7	3	0.167	1–2	330	4500	228	36.2	1018–2105
Ma et al. [14]	12	CFRP	400	114	2	57	3.51	0.167	1–2	236.9	3425	232	14.15–42.44	654.11–1429
Ding et al. [15]	12	CFRP	900	299–305	2.94–3.01	77.5–81.5	3.68–3.87	0.167	1–3	311	3481	245	32.24–48.98	4498–7407
Deng et al. [16]	2	CFRP	500	165	2	82.5	3.03	0.167	2	275	2878	244	31.2	1949
Zhao et al. [17]	24	CFRP	510	255	1.37–2.54	100.4–185.4	2.0	0.151	1–2	272–302.5	4050	257	28.72–47.95	2821–4453
Cao et al. [18]	2	CFRP	400	133	4	33.3	3.01	0.12	2–4	340	2471	210	140.3	2628–3342
	2	GFRP	400	133	4	33.3	3.01	0.169	2–4	340	1582	79	140.3	2662.16–3646.06
Shen et al. [19]	7	CFRP	450	140	6.0	23.3	3.21	0.167	1–5	240.8–348.6	3510	234	20.9	2007–2594.4
Liu et al. [20]	19	CFRP	600–780	200–260	2	100–130	3	0.167	2–5	299	3512	246	58.4–80.6	4127–6558
Zhang et al. [21]	4	CFRP	400	114	2	57	3.51	0.167	1–2	433	3425	232	16.34–29.98	955.71–1126.67
Zeng et al. [22]	3	CFRP	600	219	6	36.5	2.74	0.167	2	315.2	4324.2	233	42.47	3643.5–4113.5
Xiong et al. [23]	4	CFRP	300	85–87	2–3	42.5–29	3.45–3.53	1.4	2–3	330	1800	228	25	573–840
Zhang et al. [24]	4	CFRP	636	159	4	39.8	4	0.167	1–4	466.5	4306.4	269	32.4	2225–3300
Sun et al. [25]	6	CFRP	400–600	132.5–133.3	4.5	29.4–29.6	3–4.5	0.111	1–2	360	4900	228	53.6	2010–2264
Alwash et al. [26]	2	CFRP	300	100	2	50	3	0.131	1	335	4300	234	23.5	760–591
Wang et al. [27]	10	CFRP	400	127–136	1.5–6	22.7–87.7	2.94–3.15	0.167	1–2	310–350	4900	230	41.8–44	1086–2186
Ma et al. [28]	12	CFRP	200	100	2.5–3.5	28.6–40	2	0.167	1–3	386	3961	240	64.1–84.3	1412.5–2129.5
	12	GFRP	200	100	2.5–3.5	28.6–40	2	0.17	1–3	386	2200	100	64.1–84.3	1202–1694
Gu et al. [29]	10	CFRP	400	127–136	1.5–6.0	22.7–84.7	2.94–3.15	0.167	1–2	310–350	1260	230	40.15	1294–1886
Na et al. [30]	1	CFRP	588	168	6	28	3.5	0.111	2	243	3550	250	38	2360
Yu et al. [31]	2	GFRP	400	202–204	1–2	102–202	1.96–1.98	0.169	1–3	226–231	1825	80	37.1–45.6	1283–1593
Abdalla et al. [32,33]	18	GFRP	250–350	114–167	3.1–5.6	20.4–53.9	2.1–2.19	0.352	1	350	3400	72	36.53–51.43	1241–2124
Hu et al. [34]	9	GFRP	400	202–204	1–2	102–202	1.98	0.17	1–4	226–242	1825.5	80.10	35.9–42.2	1710–2561
Teng and Hu [35]	3	GFRP	450	165	2.75	60	2.73	0.17	1–3	385	1825.5	80.10	43.80	1460–1500
Total	**252**	**Max**	**900**	**305**	**7.5**	**202**	**4.5**	**0.352**	**5**	**466.0**	**4900**	**269**	**140.30**	
		Min	**200**	**85**	**1.0**	**17.73**	**1.96**	**0.111**	**1**	**226**	**1260**	**79**	**14.15**	

Table 2
Geometric and material properties of tests on FRP-confined square CFST short columns.

Ref.	No.	FRP Type	Geometrical properties							Material Properties				$P_{u\text{-}Exp}$ (kN)
			L (mm)	D (mm)	t_s (mm)	D/t	L/D	t_f (mm)	n_f	Steel f_{ys} (MPa)	FRP f_{tf} (MPa)	E_f (GPa)	Concrete f_c (MPa)	
Ma et al. [14]	10	CFRP	400	110	2	55	3.64	0.166	1–2	236.9	3425	232	14.15–42.44	501–799
Cao et al. [18]	9	CFRP	400	120	3	40	3.33	0.167	1–4	340	2471	210	38.7–140.3	1102–2303.7
	2	GFRP	400	120	3	40	3.33	0.167	2–4	340	1582	79	140.3	2244.84–2292.44
Alwash et al. [26]	2	CFRP	300	100	2	50	3	0.131	1	335	4300	234	24.2	586–617
Park et al. [36,37]	6	CFRP	550	125	3.2–6.0	20.8–39.1	4.40	0.111	1–3	311–373	3500	233	49.9	1309–1936
Wei et al. [38]	12	CFRP	400	133	3	44.3	3.01	0.111	1–4	264.4–268.4	4067.0	239	31.2–34.7	1250–1920
Wang and Shao [44]	12	CFRP	420	140	3.5	40	3	0.111	1–3	300	4570	226	22.3–40	969–1799
Wang et al. [39]	6	CFRP	420–630	140	3.5	40	3–4.5	0.111	1–3	300	4830	230	32.83	1470–1592
Liang et al. [40]	3	CFRP	600	125	6.5	19.2	4.8	0.167	1–3	248	3471	255	16.42	1067–1299
Li et al. [41]	6	CFRP	400	191	4–6	31.8–47.8	2.09	0.167	1–3	295	1500	210	53.6	2215–2775
Zhang and Xiao [42]	2	CFRP	800	300	6.0	50	2.67	0.167	4	433	3652	239	30	7281–7727
	2	GFRP	800	300	6.0	50	2.67	0.167	4	433	1429	78	30	6812–7264
Total	**72**	**Max**	**800**	**300**	**6.5**	**55**	**4.80**	**0.167**	**4**	**433**	**4830**	**255**	**140.30**	
		Min	**300**	**91.5**	**2.0**	**19.23**	**2.09**	**0.111**	**1**	**236**	**1429**	**78**	**14.15**	

mental programmes are included in the tables, including 252 experiments on confined circular CFSTs with CFRP (200 samples) or GFRP (52 samples) and 72 tests on confined square CFSTs (68 with CFRP and 4 with GFRP) [7–44]. The tests included a range of different concrete strengths. In accordance with the guidance given in EN 1992–1–1 [55], in the current work, concrete with a compressive strength $f_c \leq 50$ MPa is defined as NSC, HSC is defined as 50 MPa $\leq f_c \leq$ 90 MPa whilst for UHSC $f_c >$ 90 MPa. It is noteworthy that some test programmes reported the cubic concrete strength (f_{cu}), and these were converted to f_c values herein using Eq. (1) as suggested by Mirza and Lacroix [56], where both f_c and f_{cu} are in MPa:

$$f_c = \left[0.76 + 0.2\ log_{10}\left(\frac{f_{cu}}{19.6}\right)\right] f_{cu} \tag{1}$$

As shown in Tables 1 and 2, the range of concrete compressive strengths examined in these tests was between 14.15 and 140.39 MPa. The carbon steel tubes had a yield strength f_{ys} of between 226 and 466.5 MPa, whilst the yield strength of the FRPs (f_{tf}) was between 1260 and 4900 MPa for the CFRP and 1582 to 3400 MPa for the GFRP. The thickness of the CFRP and GFRP layers ranged from 0.11 to 0.234 mm and from 0.169 to 0.352 mm, respectively. It has been shown that the slenderness ratio has an important role in the axial compressive strength of FRP-confined CFSTs [9,25,36-37,51-52]. In the tests examined herein, the D/t ratio varied between 17.73 and 200 for the circular tubes and 19.23 to 50 for the square cross-sections. On the other hand, short columns are classified as those with a length to depth/diameter ratio (L/D) of less than or equal to 5 [57,58]; all of the specimens examined herein had a L/D ratio of between 1.96 and 4.50.

3. Existing design models

As stated before, a number of different analytical design solutions have been proposed for the prediction of the ultimate resistance of FRP-confined circular and square CFSTs. These are summarised in Tables 3 and 4 for FRP-confined CFSTs with a circular and square cross-section, respectively. In this table, P_i indicates the ultimate design strength, where the subscript i varies depending on the reference article. It is worth noting that the notation used in Tables 3 and 4 have been changed in some cases from those employed in the original source reference, for ease of comparison. From the expressions given in the tables, it is clear that there are the two main influential parameters included in almost all approaches, and these are the steel tube confinement index ξ_s and the FRP confinement index ξ_f, these are defined in Eqs. (2) and (3), respectively:

$$\xi_s = \frac{A_s f_y}{A_c f_c} \tag{2}$$

$$\xi_f = \frac{A_f f_f}{A_c f_c} = \frac{4E_f t_f \varepsilon_f}{f_c D} \tag{3}$$

where A_s A_c and A_f are the cross-sectional areas of the steel tube, concrete core and FRP wrapping, respectively and ε_f is the ultimate tensile strain of the FRP. It is worth noting that all of the design models employ the gross cross-sectional area of the steel tubes because local buckling does not occur before the ultimate load has been reached owing to the FRP wrapping. In addition, in all expressions given in Tables 3 and 4, ξ_s and ξ_f are determined as given in Eqs. (2) and (3), respectively.

4. Reliability index for the design models

The reliability index β provides a comparative measure of the reliability of a component or structure and is generally used to determine the probability of failure. Based on the first-order probabilistic theory and the hypothesis that the design resistance (P_i) and load effects have log-normal distributions, β [59,60] is determined in accordance with Eq. (29):

$$\beta = \frac{Ln\left(\frac{P.M.F}{\varphi}\right)}{\alpha\sqrt{V_M^2 + V_P^2 + V_F^2}} \tag{29}$$

Table 3
Summary of selected design resistances of FRP-confined circular CFST short columns [7,9-15,28,32,43,45].

Ref	FRP type	Design resistance, P_i	Formula number
Ding, et al. [15]	CFRP	$P_{Ding} = (1 + 1.7\xi_s + 1.7\xi_f)f_{ck2}A_c$ where: $f_{ck2} = 0.4f_{cu}^{(7/6)}$	(4)
Wei, et al. [7]	CFRP and BFRP	$P_{Wei} = A_{cs}f_{csf}$ where: A_{cs} is the total cross-sectional area of the CFST column and $f_{csf} = (1 + 1.27\xi_s + 1.28\xi_f)f_c$	(5) (6)
Lu, et al. [12]	CFRP and GFRP	$P_{Lu.2014} = (1 + 1.8\xi_s + 1.15\xi_f)A_cf_c$	(7)
Lu, et al. [45]	CFRP and GFRP	$P_{Lu.2016} = \begin{cases} (1 + 2\xi_s + 1.36\xi_f)A_cf_c & 0 \le \xi_s \le 1.235 \\ (1 + 1.1\xi_s + \sqrt{\xi_s} + 1.36\xi_f)A_cf_c & \xi_s > 1.235 \end{cases}$	(8)
Che, et al. [13]	CFRP	$P_{Che} = (1.14 + 1.02(\xi_s + 3\xi_f))A_{sc}(f_{ck})$ A_{cs} is the total cross-sectional area, in this case neglecting the area of the FRP A_f $f_{ck} = 0.67f_{cu}$	(9)
Tao, et al. [10]	CFRP	$P_{Tao} = (1 + 1.02\xi_s)A_{sc}f_c + 1.15\xi_f f_c A_c$	(10)
Ma, et al. [14]	CFRP	$P_{Ma2022} = \left(1 + 0.144\xi_f\frac{f_c}{f_{c30}}\right)\left(1 + 0.069\sqrt{\xi_s} + 1.142\xi_s\right)A_cf_c$	(11)
Park, et al. [9]	CFRP	$P_{Park} = A_sf_y + A_cf_{cc}$ where: $\frac{f_{cc}}{f_c} = 1 + 2.86\frac{f_{rp}}{f_c}$ $f_{rp} = \frac{2f_{ys}t_s + 2f_ft_f}{D_c}$ D_c = Diameter of infill concrete	(12) (13) (14)
Ma, et al. [28]	CFRP and GFRP	$P_{Ma.2023} = A_{sc}f_{ck}\left(1 + \frac{12q_s}{f_{ck2}}\right) + 109n_f^{0.9}f_{co}A_{sc}\left(\frac{f_{rp}}{f_c}\right)^{2.06}$ where: $f_{rp} = \frac{2K_2E_f\varepsilon_ft_f}{D_c}$ D_c = Diameter of the infill concrete k_2 = 0.54 and 0.52 for CFRP and GFRP, respectively, $q_s = \frac{k_sA_sf_y}{2A_c}$ k_s = 0.3, and $f_{ck2} = 0.4f_{cu}^{(7/6)}$	(15) (16)
Dong, et al. [43]	CFRP	$P_{Dong} = A_sf_y + A_cf_c(0.95 + f_1 + min(f_2, f_3))$ where: $f_1 = 0.49\left(\frac{A_sf_{ys}}{A_cf_c}\right)^{0.51}$ $f_2 = 0.00085(E_l)^{0.8}(f_c)^{-0.29}$ $f_3 = 0.6(\varepsilon_fE_l)^{0.86}(f_c)^{-0.59}$, and $E_l = \frac{2E_ft_f}{D_c}$	(17) (18a) (18b) (18c)
Cao, et al. [18]	CFRP and GFRP	$P_{Cao} = (1 + 1.02\xi_s)A_{sc}f_c + 1.78\xi_fA_sf_c)$	(19)
Abdalla, et al. [32]	GFRP	$P_{Abdallah} = A_sf_y + A_cf_c + k\left(\frac{2f_yt_s}{D} + \frac{2f_ft_f}{D}\right)$ where: $k = 4$	(20)

In this expression, the design resistance P is taken as the average ratio of $\left(\frac{P_{ul-Exp}}{P_i}\right)$, where P_{ul-Exp} is the experimental design resistance and P_i is the design resistance (i varies depending on the source document); M is the average ratio of the measured-to-nominal material yield strengths and is assumed to have a value equal to 1.10; F is the average ratio of the measured-to-nominal dimensions of the cross-section and is assumed to have a value of 1.00; and the sensitivity factor for resistance (α) is taken as 0.70. For the other terms in the expression, $V_F = 0.05$ (coefficient of variation of F), $V_M = 0.1$ (coefficient of variation of M), φ is a resistance factor which is taken as 0.75 and the coefficient of variation of P is V_P. The same methodology has been employed elsewhere [61–64] for analysing the reliability of design models for different concrete-filled steel tubular columns. However, the parameter values used in Eq. (29) followed the analysis made by Chen [64] for CFST columns. This is because the safety of designed structures is mostly achieved by first order probabilistic theory. Separate load and resistance factors are applied to specified load effects and nominal resistances, to ensure that the limit state is not violated. Accordingly, the load effects are based on the combination of dead and live loads, which are independent of the cross-section shape. With regard to the resistance uncertainties, all of the materials (FRP, steel tube and concrete) are considered to have an average ratio of the measured-to-nominal material strengths of 1.10. Based on this assumption, the input data used for CFST columns has been employed herein for FRP-confined CFST columns. The target reliability index is 3.0 because failure of FRP-confined CFST columns can be classified as sudden, according to ASCE [65]. This is because the typical failure mode for these columns is caused by rupture of the FRP wrapping in the mid-height region. Further discussion on this is given elsewhere [12]. On the other hand, a recent study by Zarringol et al. [80] showed that the most influential parameter on the behaviour of FRP-confined CFST columns is the slenderness of the steel tube. Accordingly, this parameter, expressed as the D/t ratio, was employed as the main parameter in their reliability analysis [80] and also in the current work.

5. Assessment of different design approaches

This section evaluates the accuracy of the design resistance P_i

Table 4
Summary of selected design resistances of FRP-confined square CFST short columns [14,38,42,18,44].

Ref	FRP type	Design resistance, P_i	Formula number
Ma, et al. [14]	CFRP	$P_{Ma2022} = \left(1 + 0.22\xi_f \frac{f_c}{f_{c30}}\right)\left(1 + 0.556\sqrt{\xi_s} + 1.311\xi_s\right)A_c f_c$	(21)
Wei, et al. [38]	CFRP	$P_{Wei} = A_{csf} f_{csf}$ where:	(22)
		$f_{csf} = \left(1 + 1.27\xi_s\left(0.787 + 0.213\left(\frac{2r}{B}\right)\right) + 1.28\xi_f\left(\frac{2r}{B}\right)^{1.82}\right)f_c$ and	(23)
		r = corner radius, 15 mm	
Zhang and Xiao [42]	CFRP and GFRP	$P_{Zhang} = A_s f_y + f_{cc} A_c$ where:	(24)
		$f_{cc} = f_{co}\left(0.5 + 1.225\left(\frac{f_{rp}}{f_c}\right)^{0.6}\right)$	(25)
		$f_{rp} = \frac{2f_{ys}t_s + 2f_f t_f}{B_c}$ and	
		B_c = Width of the infill concrete	
Cao, et al. [18]	CFRP and GFRP	$P_{Cao} = (1 + 1.02\xi_s)A_{sc} f_c + 0.729\ \xi_f A_s f_c)$	(26)
Wang and Shao [44]	CFRP	$P_{Wang} = A_{csf} f_{csf}$ where:	(27)
		$f_{csf} = [1.18 + 0.85(\xi_f + \xi_s)]f_{ck}$ and	(28)
		$f_{ck} = 0.67 f_{cu}$	

determined using different approaches in comparison to the ultimate test resistance $P_{ul\text{-}Exp}$, where the subscript i refers to the first author of the design approach under consideration as provided in Tables 3 and 4. The data is presented in Figs. 2 and 3 in terms of the ratio of $P_i/P_{ul\text{-}Exp}$ versus the slenderness ratio, for the FRP-confined circular and square CFST columns, respectively. Linear trend lines are also included in the figures to illustrate the accuracy of different design techniques across the entire slenderness range. It is noteworthy that the slenderness presents that of the circular steel section or the square steel section without considering the FRP (i.e. the ratio of D to t_s). The assessment of the different design approaches is made in the following subsections for CFRP-confined circular CFST columns, GFRP-confined circular CFST columns and FRP-confined square CFST columns, respectively. First, the design resistance of the specimens was calculated with different numerical models P_i and compared with the corresponding test result $P_{ul\text{-}Exp}$.

5.1. CFRP-confined circular CFSTs

This section presents a comparison between the test resistances and those obtained from the available design models for CFRP-confined circular CFST columns, as presented in Table 3. The results are given in Table 5 which provides the $P_i/P_{ul\text{-}Exp}$ values, where the average (Avg), standard deviation (SD), maximum ratio value (Max) and minimum ratio value (Min) are also provided. The reliability index β is also presented in the table for the different design models. It is noteworthy that this table also includes the results from a new design method, which is proposed later in this paper, in Eq. (36).

As evident from the data in Table 5, most of the design models provide conservative resistances with the $P_i/P_{ul\text{-}Exp}$ ratios ranging between 0.70 and 0.99. The most conservative predictions are obtained using the models proposed by Cao, et al. [18], Ma, et al. [14] and Dong, et al. [43]. It is noteworthy that the design model by Ma, et al. [14] is based on an advanced machine learning algorithm, which appears to implement a high safety factor, while the highly conservative predictions of Dong, et al. [43] may result from the conservative numerical analyses used in their study. The model proposed by Tao, et al. [10] includes the contribution made by the FRP to increasing the strength of the infill concrete ($1.15\xi_f f_c A_c$), as does this models of Ma, et al. [28] and Cao, et al. [18] although these yield slightly more conservative results. It is noteworthy that the models of Ma, et al. [28] and Cao, et al. [18] were initially proposed for CFRP-confined circular CFST columns filled with HSC and UHSC, respectively. Overall, the most accurate estimations of the ultimate strengths comes from the design models proposed by Wei, et al., [7] and Lu, et al. [45] with an average $P_i/P_{ul\text{-}Exp}$ ratio of 1.03. On the other hand, the model of Park, et al. [9] provides the most unconservative predictions with an average $P_i/P_{ul\text{-}Exp}$ ratio of 1.23, which may be attributed to the small number of specimens used in their design equation proposal (only 11 specimens were used).

The degree of scatter within the predictions obtained by different design models is relatively high as demonstrated by the standard deviation, SD, values in the range of 0.116 to 0.218, with the exceptions of the design models proposed by Tao, et al. [10], Che, et al. [13], Ma, et al. [14] and Cao, et al. [18] which had SD values ranging between 0.095 and 0.107. With regard to the reliability index β, all of the design models assessed herein resulted in an acceptable reliability (β>3.0) as indicated by the bold font in the table, apart from the models proposed by Ding, et al. [15], Park, et al. [9] and Lu, et al. [45].

The relationship between $P_i/P_{ul\text{-}Exp}$ and the column slenderness D/t for the different design models is presented in Fig. 2 with a trend line included to observe the average and general behaviour. It is noteworthy that the figures are plotted using the column slenderness D/t because it is the main factor influencing the confinement of concrete within it. Accordingly, using other parameters such as the concrete strength or FRP confinement level may lead to other outcomes, and this warrants further investigation in the future. For these plots, as the slope of the trend line reduces, the accuracy of the design method under consideration, increases. Generally, the design models of Ding, et al. [6], Lu, et al. [12], Ma, et al. [28] and Lu, et al. [45] show reducing accuracy for relatively lower values of D/t when $P_i/P_{ul\text{-}Exp} \leq 1$. On the other hand, when the design model presents unconservative resistance predictions (i.e. $P_i/P_{ul\text{-}Exp} > 1$), a relative increase of the slenderness of the steel tube results in a more unconservative prediction, as demonstrated by Park, et al. [9]. However, the design models proposed by Wei, et al. [7] and Cao, et al. [18] provide a similar level of accuracy over the entire D/t ratio range examined herein. Based on the above discussions, it is determined that the design model by Wei, et al. [7] can be used in design, despite being slightly unconservative on average. However, overall, the data presented in this section following a detailed analysis of the available design methods for a variety of parameters shows that a new, more accurate, design method would be beneficial.

5.2. GFRP-confined circular CFSTs

This section presents a similar analysis as in the previous section but for GFRP-confined CFSTs rather than those with CFRP as in Section 5.1. As such, Table 6 presents the average ratios of the analytical design resistance of GFRP-confined circular CFSTs to the experimental resistance $P_i/P_{ul\text{-}Exp}$, together with the standard deviation (SD), maximum

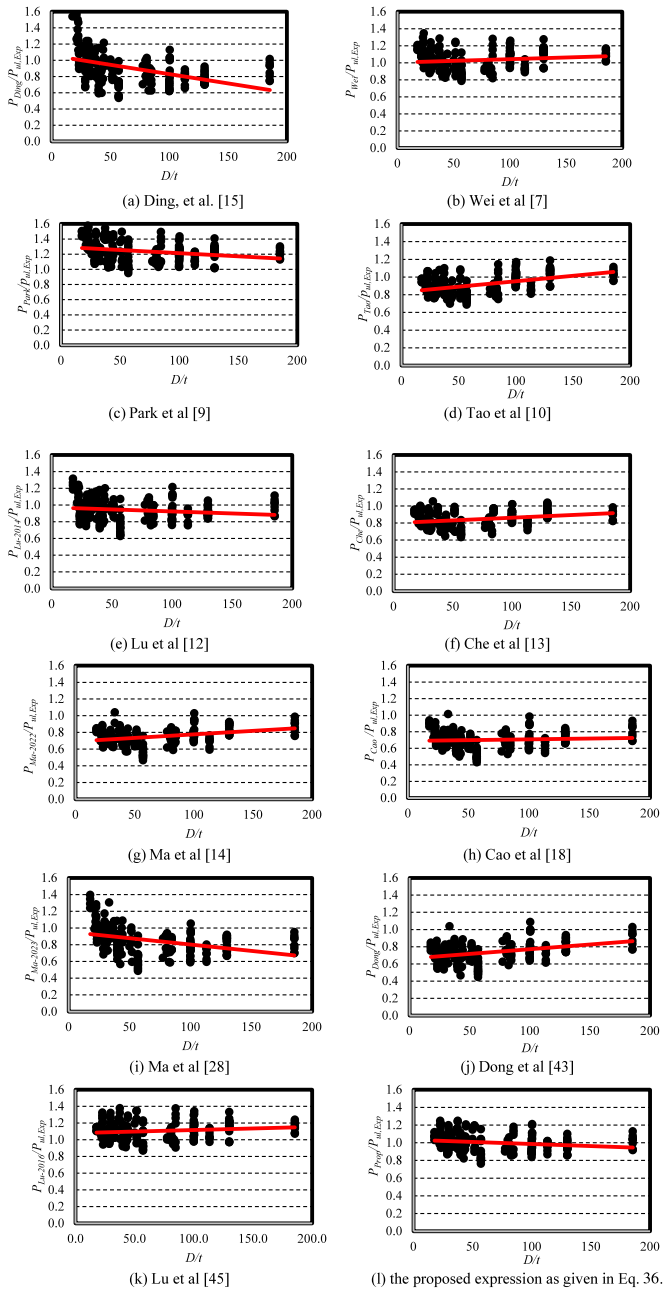

Fig. 2. $P_i/P_{ul\text{-}Exp}$ versus D/t for the different design models for CFRP-confined circular CFST short columns.

ratio value (Max), minimum ratio value (Min) and reliability index (β) for each design method. It is observed that all of the design methods examined herein result in conservative predictions of the ultimate resistance, with the method proposed by Abdallah, et al. [32] giving the most highly conservative predictions (Avg=0.64). Additionally, the scatter of the predictions obtained by the different design models is relatively high (SD in the range of 0.167 to 0.176), except for the design model of Abdallah, et al. [32] which provides a relatively low standard deviation value of 0.097. The most accurate design expression is the method proposed by Lu, et al. [12], as it was for the CFRP-confined specimens, although this method resulted in an unacceptable reliability index value (i.e. β <3.0).

In addition, Fig. 3 presents the $P_i/P_{ul\text{-}Exp}$ versus column slenderness D/t values for the different design models, with a trend line included to observe the average and general behaviour. Generally, it is observed that of all the analytical models exhibit reducing levels of accuracy for specimens with a relatively high D/t ratio. Hence, as for the CFRP-confined specimens previously assessed, it is concluded that a new design model which provides more accurate and reliable results, with less scatter for a range of realistic slenderness values, is required.

5.3. CFRP-confined square CFSTs

In accordance with the test details presented in Table 2, for the tests on FRP-confined CFSTs with a square cross-section, all but four of the available experiments employed carbon FRP for the wrapping whilst the remained used GFRP. Therefore, the analysis presented herein focuses only on square sections tests with CFRP, as there is insufficient data for those with GFRP. Table 7 presents the average design capacity to experimental ultimate load ratio ($P_i/P_{ul\text{-}Exp}$) for each of the design methods presented in Table 4, together with the standard deviation (SD), maximum ratio value (Max), minimum ratio value (Min) and reliability index (β). It is observed that the design method proposed by Ma, et al. [14] and Zhang and Xiao [42] provide unconservative resistance values, as the $P_i/P_{ul\text{-}Exp}$ ratios ranged between 1.12 and 1.28. Additionally, the scatter of the predictions obtained by the different design models is relatively high, ranging between 0.141 and 0.252. Regarding the reliability index β, all the design methods provide an acceptable level of reliability except for those proposed by Ma, et al. [14] and Zhang and Xiao [42].

The relationship between $P_i/P_{ul\text{-}Exp}$ and section slenderness D/t is presented for each design method in Fig. 4. It is clear from these graphs that there is a large variation in accuracy for the design methods for different geometric configurations. This is observed for all levels of slenderness examined in the experimental programmes and highlights the need for a new, more accurate and reliable design procedure for the determination of the ultimate strength of FRP-confined short CFST columns.

6. Confinement-based direct design model

The confinement-based direct design method is a new design model for short CFST columns developed originally by Hassanein and Silvestre [62] for single and double-skin rubberised CFST columns. It has been extended a number of times to incorporate different geometries of concrete-filled columns [66–69]. The method employs available databases of experimental results for particular cross-sections to derive a formula for the lateral confining stress (f_{rp}) of the concrete core. Then, the f_{rp} expression is used to determine the resistance of the cross-section based on the sum of the resistances of the different cross-sectional components (i.e. the concrete core and steel tube for CFST). In the current work, this method is further extended to account for the effect of the FRP confinement on the overall capacity, as shown in Fig. 5. Unlike the concrete in CFST columns, in this case both the FRP and the steel tube contribute to the confinement provided to the concrete core. It is also noteworthy that while the confinement for circular concrete is uniform, this is not the case for square cross-sections, where confinement can be more concentrated in the corner regions [15,36-38,40-44,51]. Therefore, to simplify this issue, for square columns sections, the average confining stress is employed for design purposes.

6.1. Calculation of the lateral confining stress f_{rp}

The first step to providing a general design model that can accurately estimate the design resistance of FRP-confined circular or square CFST short columns is to calculate the lateral confining stress (f_{rp}). It is this pressure that increases the effective concrete strength in a filled steel tube from the compressive strength f_c to f_{cc}, which is the confined concrete strength. Herein, the modified formula given by Liang [70] is adopted, as follows:

$$f_{cc} = \left(\gamma_c f_c + k f_{rp}\right) \tag{30}$$

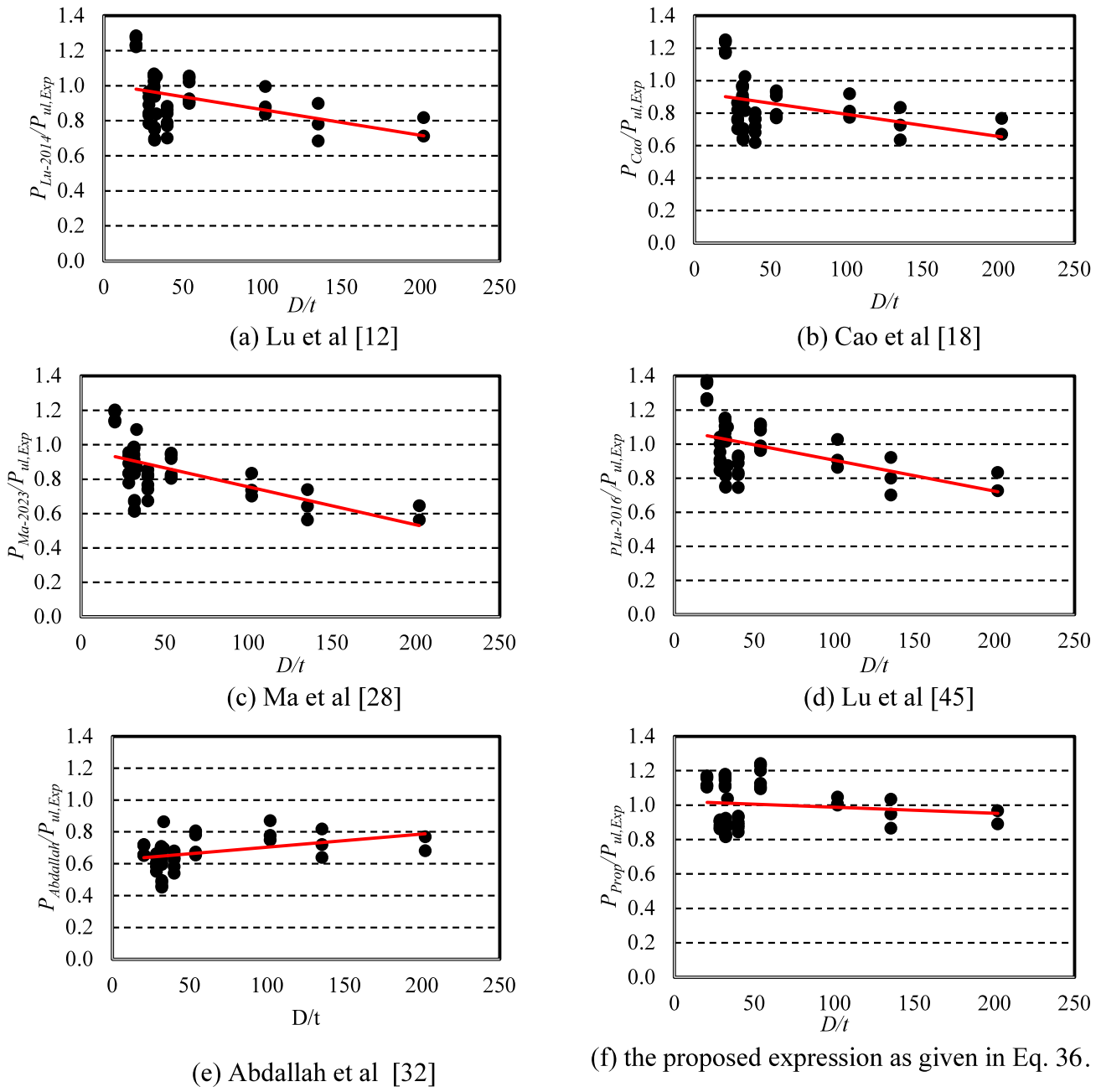

Fig. 3. $P_i/P_{ul\text{-}Exp}$ versus D/t for the different design models for GFRP-confined circular CFST short columns.

where k is a confinement coefficient (triaxial factor) which depends on the degree of confinement and γ_c is given by Eq. (32). Many of the different design methods which have been proposed for concrete filled tubular members are based on the expression developed by Richart, et al. [71], and typically differ in the determination of the coefficient k. Some approaches adopt a linear relation between the compressive stress of the concrete core (f_c) and the lateral pressure (f_{rp}), while others are nonlinear. Richart, et al. [71] proposed a value of k equal to 4.1 for circular CFST short columns filled with NSC, while Cederwall [72] assumed a value of between 3 and 4 for CFSTs filled with HSC. The

Table 5
$P_i/P_{ul\text{-}Exp}$ ratios using the various design models for CFRP-confined circular CFST short columns.

	P_{Ding} Eq. 4 [15]	P_{Wei} Eq. 5 [7]	P_{Park} Eq. 12 [9]	P_{Tao} Eq. 10 [10]	P_{Lu2014} Eq. 7 [12]	P_{Che} Eq. 9 [13]	P_{Ma2022} Eq. 11 [14]	P_{Cao} Eq. 19 [18]	P_{Ma2023} Eq. 15 [28]	P_{Dong} Eq. 17 [43]	P_{Lu2016} Eq. 8 [45]	Proposed Equation Eq. (36)
Avg	0.90	**1.03**	1.23	0.91	**1.03**	0.86	0.75	0.70	0.85	0.74	1.11	**1.00**
SD	0.218	0.116	0.143	0.109	0.107	0.095	0.102	0.106	0.172	0.117	0.112	0.103
Max	1.74	1.34	1.63	1.19	1.26	1.05	1.04	1.01	1.40	1.09	1.38	1.24
Min	0.54	0.79	0.95	0.69	0.80	0.63	0.47	0.43	0.49	0.45	0.87	0.76
β	2.74	**3.33**	1.82	**4.04**	**3.41**	**4.56**	**4.29**	**4.15**	**3.05**	**3.89**	2.88	**3.68**

Table 6
$P_i/P_{ul\text{-}Exp}$ ratios using the various design models for GFRP-confined circular CFST short columns.

	P_{Lu2014} Eq. 7 [12]	P_{Cao} Eq. 19 [18]	P_{Ma2023} Eq. 15 [28]	P_{Lu2016} Eq. 8 [45]	$P_{Abdallah}$ Eq. 20 [32]	Proposed Equation Eq. (36)
Avg	0.93	0.86	0.86	**0.99**	0.64	**1.00**
SD	0.167	0.169	0.170	0.176	0.097	0.131
Max	1.28	1.25	1.20	1.37	0.86	1.24
Min	0.68	0.62	0.56	0.70	0.43	0.82
β	**3.13**	**3.35**	**3.05**	2.84	**4.30**	**3.27**

Table 7
$P_i/P_{ul\text{-}Exp}$ ratios using the various design models for CFRP-confined square CFST short columns.

	P_{Ma2022} Eq. 211 [14]	P_{Wei} Eq. 22 [38]	$P_{Zhang\ and\ Xiao}$ Eq. 24 [42]	P_{Cao} Eq. 26 [18]	$P_{Wang\ and\ Shao}$ Eq. 27 [44]	Proposed Equation Eq. (36)
Avg	1.28	**0.95**	1.12	**0.97**	1.03	**0.99**
SD	0.165	0.141	0.252	0.144	0.157	0.092
Max	1.66	1.30	1.98	1.31	1.44	1.18
Min	1.06	0.73	045	0.76	0.79	0.84
β	1.47	**3.51**	1.62	**3.40**	**3.01**	**3.95**

majority of the analytical models presented and assessed in the current paper utilise the ultimate stress of the FRP, as determined from a tensile test on a coupon, to calculate the confining lateral pressure. The model proposed by Park, et al. [9] recommends a value of 2.86 for k for CFRP-confined circular CFST short columns based on the resistance models for fibre-reinforced plastic-confined concrete proposed by Lam and Teng [73]. In addition, Teng, et al. [35,54] proposed using the formula given in Eq. (30) with a value of k equal to 3.5 for CFRP and GFRP-confined stainless steel CFST short columns. Moreover, Matthys, et al. [74] proposed a value of k equal to 2.3 based on large-scale experiments on FRP-confined circular concrete columns and Soman and Chandrakumar [47] recommended a value for k equal to 0.93 for CFRP-confined square CFST columns.

Based on the above review of the confinement coefficient (k), it is important to examine its value using the full database of results and information. Accordingly, k has been calculated using the formula suggested by Park, et al. [9], as presented by Eq. (39). This equation was originally developed for the confinement provided by a steel jacket and is given as:

$$\frac{f_{cc}}{f_c} = 2.25\sqrt{4.9\left(\frac{f_{rp}}{f_c}\right) - 2\frac{f_{rp}}{f_c} - 1.25} \tag{31}$$

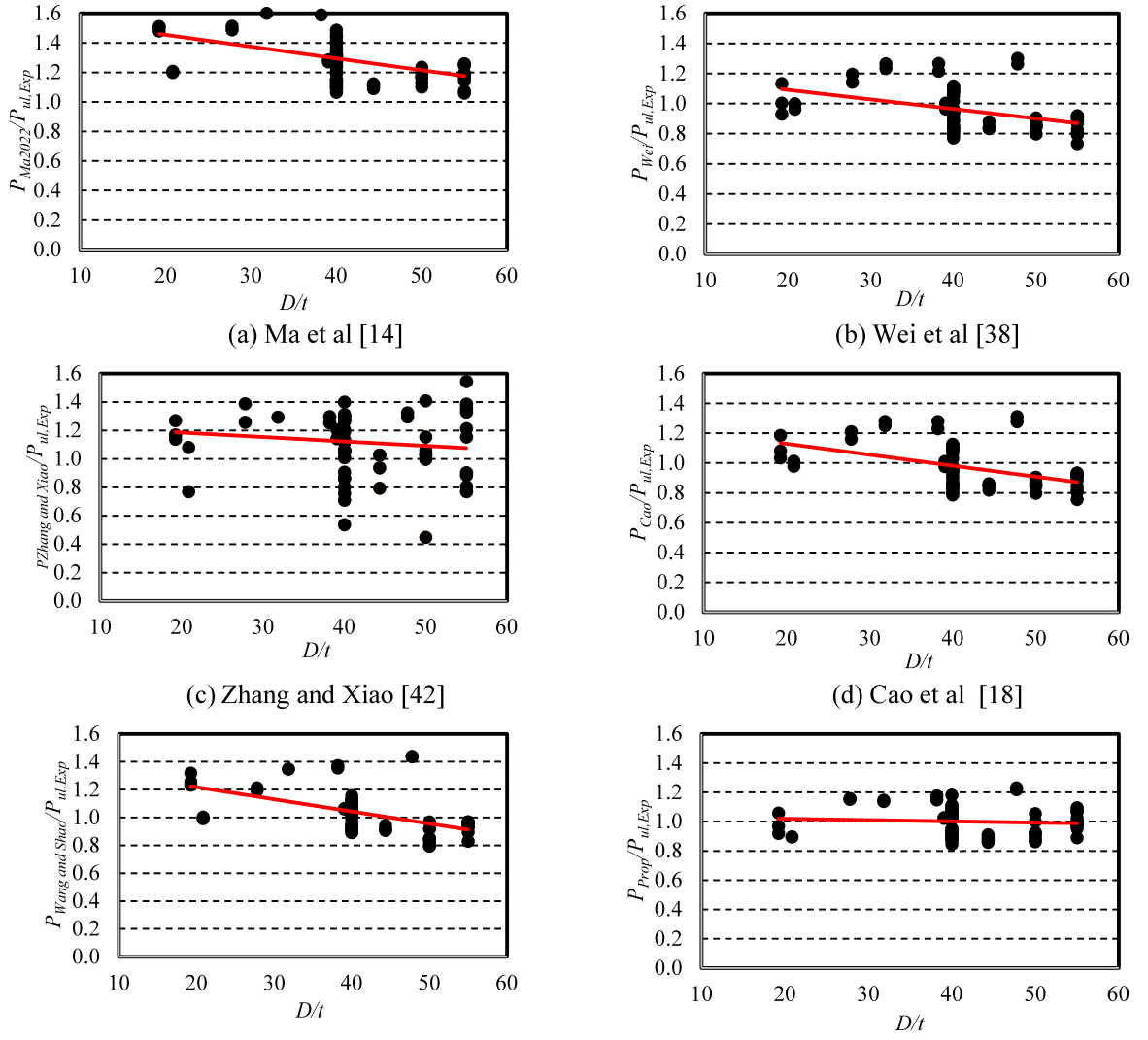

Fig. 4. $P_i/P_{ul\text{-}Exp}$ versus D/t for the different design models for CFRP-confined square CFST short columns.

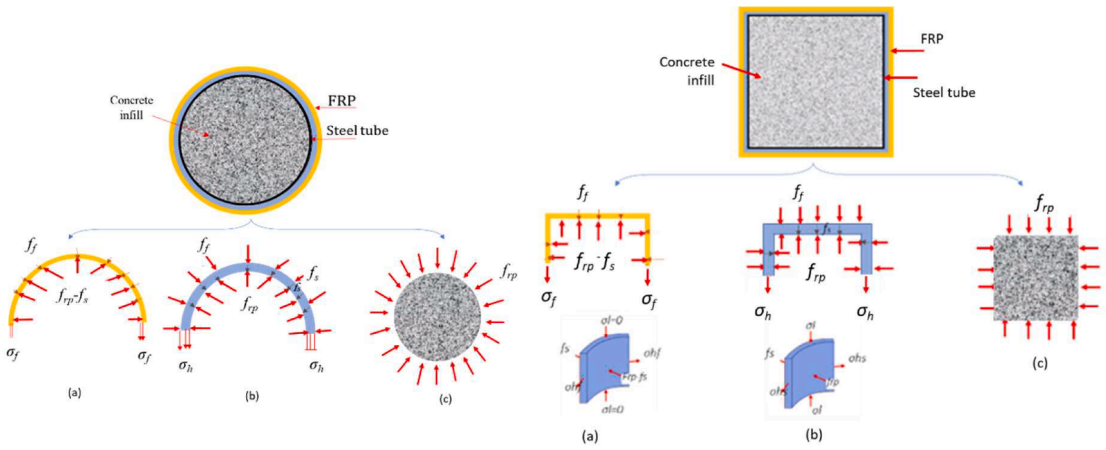

Fig. 5. Illustration of the different components of the confining stress acting on the concrete core of FRP-confined circular and square CFST short columns, including from (a) the FRP, (b) the steel tube and (c) acting on the concrete core.

where f_{rp} is the lateral confining pressure which is calculated elsewhere [9,34,35] using the expression given in Eq. 14 in Table 3 employed to determinef_{rp} $\left(\text{i.e. } f_{rp} = \frac{2f_{ys}t_s+2f_ft_f}{D_c}\right)$. The relationship between $\frac{f_{cc}}{f_c}$ and $\frac{f_{rp}}{f_c}$ is presented in Fig. 6. The slope of the obtained relationship (given by the red dashed line) reveals that the confinement coefficient has a value of 2.86, which is similar to the value obtained by Park, et al. [9]. Accordingly, this value is used in further analyses.

According to Liang [70], the factor γ_c depends on the diameter of the concrete core (D_c), and is given as:

$$\gamma_c = 1.85D_C^{-0.135}\ 0.85\ \leq \gamma_c \leq 1.0 \tag{32}$$

According to previous studies [9,28,43], the confinement pressure is affected by the slenderness ratio of the steel tube (D/t), the tensile strength of the FRP (f_{tf}) and the yield strength (f_{ys}) of the steel tube. Therefore, in the current work, each of these parameters is taken into account to derive an expression for the average lateral confining pressure (f_{rp}) acting on the concrete (as shown in Fig. 5). Firstly, for each of the tests in the experimental database [7–44], Eq. (33) is employed to determine a value for f_{cc} by taking the ultimate strength P_u as equal to the test value $P_{ul,Exp}$. It is noteworthy that despite the steel tube experiencing a combination of axial compression and lateral tension due to the lateral expansion of the concrete core [75], Eq. (33) uses the yield stress of the steel tube without any reductions, in accordance with the European specifications [76]:

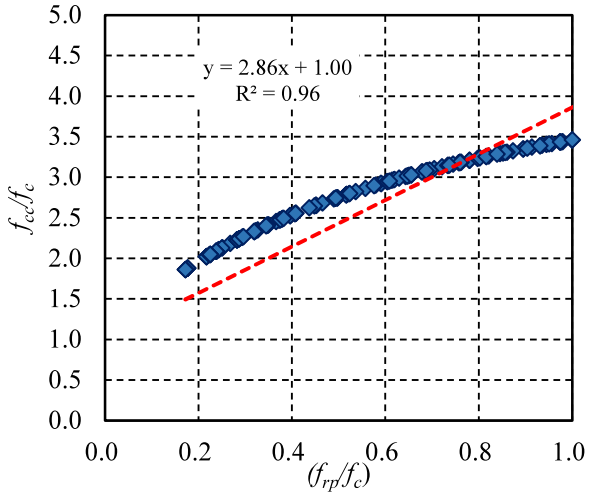

Fig. 6. Determination of the coefficient of confining k, based on the current database.

$$P_u = A_s f_{ys} + A_c f_{cc} \tag{33}$$

It has been described elsewhere in this paper, and by other researchers (e.g. [77]), that the presence of the CFRP wrapping effectively limits the development of local buckling of the steel tube and also indirectly increases the confinement on the concrete. Hence, the influence of local buckling is typically ignored in design models, as presented in Table 3.

With reference to Eq. (33), the value determined for f_{cc} is employed together with Eq. (30) to determine f_{rp} for each test specimen, assuming a value for k equal to 2.86 for CFRP and GFRP-confined CFST columns, based on the proposal of Park, et al. [9].

Thereafter, the relationship between $\left(\frac{f_{rp}}{\sqrt{f_{ys}f_{tf}}}\right)$ and $\frac{D}{\sqrt{t\times t_f}}$ is derived, as shown in Figs. 7 and 8 for circular and square columns respectively, which includes all of the key variables which affect concrete confinement. In these expressions, f_f is the tensile strength of FRP, t is the thickness of the steel tube and t_f is the thickness of the FRP. Generally, obtaining f_{rp} for CFST columns is obtained by analysing the relationship between f_{rp}/f_y and D/t. To include different variables in the derived relation, the square root of the product of the material variables $((f_{rp}\cdot f_{tf})^{0.5}$ and $(t\cdot t_f)^{0.5})$ was proposed which ensure a dimensionless comparison. This is a similar approach to that used elsewhere for the confinement-based direct design of double-skin concrete-filled columns [68]. With reference to the data presented in Fig. 7, it is observed that there is similar behaviour between the members confined with CFRP and GFRP sheets. Hence, both FRP confinement materials are consolidated into the same f_{rp} expression. Accordingly, the average value for f_{rp}, based on Fig. 7, for CFRP and GFRP-confined CFST section with a circular cross section is given by Eq. (34):

$$f_{rp} = 2.1253\left(\sqrt{f_{ys}f_{tf}}\right)\left(\frac{D}{\sqrt{t\times t_f}}\right)^{-0.929} \quad \text{For CFRP, with } R^2 = 0.746 \tag{34}$$

$$f_{rp} = 1.2022\left(\sqrt{f_{ys}f_{tf}}\right)\left(\frac{D}{\sqrt{t\times t_f}}\right)^{-0.85} \quad \text{For GFRP, with } R^2 = 0.525 \tag{35}$$

Similarly, the corresponding value for the average f_{rp}, for the CFRP-confined square columns, based on the data presented in Fig. 8, is given by Eq. (35), as there is insufficient data for those with GFRP as shown in Table 2:

$$f_{rp} = \gamma_c f_c + k\left(0.1074\left(\sqrt{f_{ys}f_{tf}}\right)\left(\frac{D}{\sqrt{t\times t_f}}\right)^{-0.642}\right) \quad \text{For CFRP, with } R^2 = 0.147 \tag{36}$$

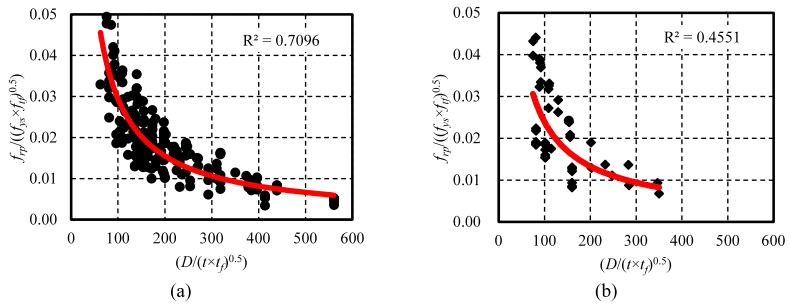

Fig. 7. Relationship between $\frac{f_{rp}}{\sqrt{f_{ys}f_{tf}}}$ and $\frac{D}{\sqrt{t\times t_f}}$ for circular CFST columns confined with (a) CFRP and (b) GFRP.

It is expected that proposing an expression for f_{rp} based on the best fit (i.e. average ratio) may result in a relatively low value of the statistical measure of fit (R^2) of the regression model, as evident in Figs. 7 and 8. However, a similar method has been successfully employed previously, in similar studies in the literature, by Schafer [78] and Gardner, et al. [79]. Accordingly, the proposed design model is carefully examined using the reliability index to overcome the relatively low value for R^2.

6.2. Proposed design resistance model

Based on the discussion in the previous section, Eq. (36) provides a general design model for the determination the design resistance of FRP-confined circular or square CFST short columns. As the main role of the FRP is to restrict lateral expansion of the member's cross-section, its contribution to the axial compressive resistance is negligible. Hence, the proposed resistance (P_{Prop}) of the column is determined as the sum of the resistances of the steel tube and the confined concrete section ($A_c f_{cc}$) where f_{cc} is determined using Eq. (30) by utilising an appropriate f_{rp} value for circular (Eq. (34), b) and square cross-sections (Eq. (35)). The expression for P_{Prop} is given as:

$$P_{prop}=\begin{Bmatrix} A_s f_{ys}+A_c\left(\gamma_c f_{cc}+k\left(2.1253\left(\sqrt{f_{ys}f_{tf}}\right)\left(\frac{D}{\sqrt{t\times t_f}}\right)^{-0.929}\right)\right) \; CFRP-Circular\ section \\ A_s f_{ys}+A_c\left(\gamma_c f_{cc}+k\left(1.2022\left(\sqrt{f_{ys}f_{tf}}\right)\left(\frac{D}{\sqrt{t\times t_f}}\right)^{-0.85}\right)\right) \; GFRP-Circular\ section \\ A_s f_{ys}+A_c\left(\gamma_c f_{cc}+k\left(0.1074\left(\sqrt{f_{ys}f_{tf}}\right)\left(\frac{D}{\sqrt{t\times t_f}}\right)^{-0.642}\right)\right) \; CFRP-Square\ section \end{Bmatrix} \quad (37)$$

where k is taken as equal to 2.86 in all cases. In the following sections, the proposed design formula is assessed and compared against test data to verify its accuracy and reliability.

6.3. Validation of the proposed method

Tables 5, 6 and 7 as well as Fig. 2(l), Fig. 3(f) and Fig. 4(f) present comparisons between the proposed design expression given in Eq. (36) with the test resistances of columns with different wrapping FRP materials and cross-sectional shapes. Overall, the proposed design expression provides a better and more reliable prediction of the ultimate capacity for CFRP- and GFRP-confined CFST short columns, demonstrated by a number of key observations:

(1) The proposed resistance results in an average $P_{Prop}/P_{ul\text{-}Exp}$ ratio of unity which is an improvement on the corresponding ratios resulting from the other design expressions presented and examined herein;
(2) P_{Prop} provides the lowest SD of all design methods examined, ranging between 0.092 and 0.104 for the CFRP-confined square and circular CFST columns;
(3) The reliability of the proposed design approach is verified as all values of β are greater than the target reliability index of 3.0;
(4) P_{Prop} is accurate for all values of steel tube slenderness examined, as demonstrated in Figs. 2(l), 3(f) and 4(f); and
(5) The accuracy of the proposed model is relatively constant (as seen in Fig. 2(l), Fig. 3(f) and Fig. 4(f)), in contrast to the other design methods examined.

However, it is noteworthy that the regression analysis was made using the test data which was employed during the model development. Accordingly, it is expected that the proposed model should perform well. On the other hand, a validation with the test resistances of columns with different wrapping FRP materials and cross-sectional shapes may increase confidence in the proposed design proposals. Accordingly, further analysis of the proposed design model is presented by comparing the results to the guidance given in Eurocode 4 Part 1–1 [76]. The design standard proposes slenderness limits of $D/t \leq 90(235/f_{ys})$ for circular short CFST columns and $D/t \leq 52((235/f_{ys})^{1/2})$ for square short CFST columns. In accordance with this, the experimental database presented in Tables 1 and 2 for FRP-confined circular and square CFST is divided into four main groups for further analysis:

(1) CFRP- and GFRP-confined circular CFST columns with $D/t \leq 90$ $(235/f_{ys})$ (Tables 8 and 9 for CFRP and GFRP, respectively);
(2) CFRP- and GFRP-confined circular CFST columns with $D/t > 90$ $(235/f_{ys})$ (Tables 8 and 9 for CFRP and GFRP, respectively);
(3) CFRP- and GFRP-confined square CFST columns with $D/t \leq 52$ $((235/f_{ys})^{1/2})$ (Table 10);
(4) CFRP- and GFRP-confined square CFST columns with $D/t > 52$ $((235/f_{ys})^{1/2})$ (Table 10)

There are a total of 156, 96, 52 and 20 individual test specimens in groups (1), (2), (3) and (4) respectively. The specimens in groups (1) to

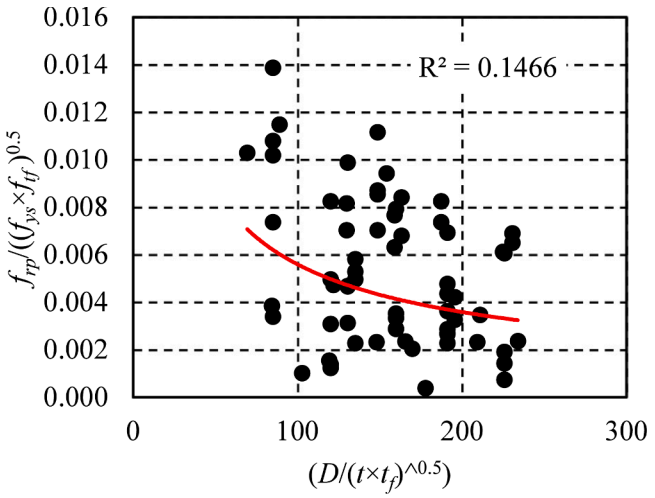

Fig. 8. Relationship between $\frac{f_{rp}}{\sqrt{f_{ys}f_{tf}}}$ and $\frac{D}{\sqrt{t\times t_f}}$ for FRP-confined square CFST columns.

(4) are each further divided into two sup-groups depending on the material grades:

(a) specimens made with normal strength steel (i.e. $f_{ys} \leq 460$ N/mm^2) and normal strength concrete (i.e. $f_c \leq 50$ MPa); and
(b) specimens made with normal strength steel (i.e. $f_{ys} \leq 460$ N/mm^2) and high strength concrete (i.e. $f_c > 50$ MPa).

As illustrated in Tables 8-10, there are no available test data for FRP-confined circular or square CFST columns with both high strength concrete (group (b)) and a high slenderness ratio. This is a notable gap in the experimental database. Nevertheless, as shown in Table 8 and 9, for CFRP-confined columns with a circular cross-section and a slenderness $D/t \leq 90(235/f_{ys})$, the design methods proposed by Wei, et al. [7], Lu, et al. [12] and the method proposed in the current paper provide the most accurate predictions on average, also with acceptable reliability indices. For the corresponding members with a relatively high slenderness value ($D/t > 90(235/f_{ys})$), only the models proposed by Tao, et al. [10] and the procedure proposed herein provide accurate predictions with acceptable reliability. On the other hand, the proposed design model in Eq. (38) is shown to be the only method of those examined to provide acceptable predictions for GFRP-confined circular CFST columns, regardless of the concrete grade used. Similar results are also observed for CFRP-confined square CFST columns, as presented in Table 10. Hence, it is concluded that the confinement-based direct design resistance approach as proposed in the current paper provides the best results in terms of accuracy and reliability of all the methods examined, for all of the criteria examined.

6.4. Assessment of a unified expression for CFRG- and GFRP-Confined CFST circular columns

This section explores if the accuracy of the predictions given in the previous section are related to the confinement level, rather than the confinement material (i.e. CFRP or GFRP). By employing the same method described in Section 6, a unified f_{rp} equation can be obtained based on the available data for all CFRG- and GFRP-confined CFST circular columns, as presented by Eq. (37):

$$f_{rp} = 1.4832\left(\sqrt{f_{ys}f_{tf}}\right)\left(\frac{D}{\sqrt{t\times t_f}}\right)^{-0.867} \text{ with } R^2 = 0.6358 \quad (38)$$

The design proposal for a CFRP- or GFRP-confined circular section is then given as:

$$P_{prop} = A_s f_{ys} + A_c\left(\gamma_c f_{cc} + k\left(1.4832\left(\sqrt{f_{ys}f_{tf}}\right)\left(\frac{D}{\sqrt{t\times t_f}}\right)^{-0.867}\right)\right) \quad (39)$$

The caparisons between the unified design method and the test strengths are presented in Tables 8 and 9, and also in Fig. 9. While the design values provide a reasonable depiction of the corresponding test values, the GFRP-confined CFST columns yielded an unacceptable reliability value (i.e. β<3.0). This may be attributed to the material properties of GFRP, which is made of less stiff fibres than CFRP. Therefore, to

Table 8
Effect of material types on $P_i/P_{ul\text{-}Exp}$ for different design approaches for CFRP-confined circular CFST short columns.

	$P_{Ding}/P_{ul\text{-}Exp}$ [15]	$P_{Wei}/P_{ul\text{-}Exp}$ [7]	$P_{Park}/P_{ul\text{-}Exp}$ [9]	$P_{Tao}/P_{ul\text{-}Exp}$ [10]	$P_{Lu2014}/P_{ul\text{-}Exp}$ [12]	$P_{Che}/P_{ul\text{-}Exp}$ [13]	$P_{Ma2022}/P_{ul\text{-}Exp}$ [14]	$P_{Cao}/P_{ul\text{-}Exp}$ [18]	$P_{Ma2023}/P_{ul\text{-}Exp}$ [28]	$P_{Dong}/P_{ul\text{-}Exp}$ [43]	$P_{Lu2016}/P_{ul\text{-}Exp}$ [45]	$P_{Prop\text{-}Eq.35}/P_{ul\text{-}Exp}$	$P_{Prop\text{-}Eq.37}/P_{ul\text{-}Exp}$	$P_{Prop\text{-}Eq.40}/P_{ul\text{-}Exp}$
		$D/t \leq 90(235/f_{ys})$												
		(a) CFRP, normal strength steel and normal strength concrete (96 specimens)												
Avg	**1.00**	**1.03**	1.29	0.88	**1.04**	0.86	0.73	0.70	0.90	0.70	1.11	**1.00**	**1.00**	**1.00**
SD	0.247	0.136	0.167	0.105	0.122	0.243	0.151	0.115	0.200	0.106	0.131	0.114	**0.112**	**0.112**
Max	1.74	1.42	1.63	1.22	1.31	2.61	1.58	0.94	1.40	0.89	1.48	1.22	**1.23**	**1.23**
Min	0.54	0.79	0.95	0.69	0.80	0.63	0.47	0.43	0.49	0.45	0.87	0.74	**0.74**	**0.75**
β	2.15	**3.10**	1.36	**4.30**	**3.16**	**3.74**	**3.86**	**3.74**	2.49	**4.03**	2.69	**3.43**	**3.45**	**3.49**
		(b) CFRP, normal strength steel and high strength concrete (22 specimens)												
Avg	0.86	**0.97**	1.15	0.84	**0.95**	0.78	0.74	0.69	0.87	0.70	1.03	**0.95**	**0.92**	0.92
SD	0.176	0.069	0.079	0.070	0.070	0.076	0.088	0.106	0.159	0.115	0.070	0.069	0.074	0.074
Max	1.14	1.17	1.28	1.08	1.13	1.05	1.04	1.01	1.31	1.04	1.19	1.11	1.10	1.09
Min	0.59	0.84	1.02	0.75	0.85	0.70	0.64	0.53	0.62	0.53	0.92	0.86	0.83	0.83
β	2.96	**4.53**	**2.83**	**5.55**	**4.69**	**5.92**	**5.66**	**4.67**	**3.33**	**4.33**	**3.96**	**4.70**	**4.77**	4.77
		$D/t > 90(235/f_{ys})$												
		(a) CFRP, normal strength steel and normal strength concrete (55 specimens)												
Avg	0.83	1.04	1.22	**0.95**	1.05	0.86	0.78	0.71	0.78	0.79	1.13	**1.00**	**1.00**	0.98
SD	0.125	0.113	0.110	0.112	0.098	0.081	0.107	0.113	0.114	0.127	0.106	0.088	0.090	0.088
Max	1.13	1.28	1.49	1.17	1.26	1.02	1.03	0.98	1.05	1.09	1.38	1.21	1.22	1.20
Min	0.62	0.82	0.99	0.75	0.85	0.72	0.56	0.50	0.59	0.51	0.91	0.86	0.84	0.83
β	**3.93**	**3.32**	2.08	**3.78**	**3.42**	**4.94**	**4.38**	**4.21**	**4.21**	**3.82**	2.78	**3.91**	**3.90**	4.05
		(b) CFRP, normal strength steel and high strength concrete (27 specimens)												
Avg	0.74	1.08	1.18	**1.01**	1.05	0.91	0.82	0.72	0.80	0.79	1.12	**0.94**	**0.92**	0.93
SD	0.069	0.093	0.104	0.082	0.084	0.066	0.060	0.063	0.093	0.068	0.097	0.059	0.069	0.060
Max	0.89	1.28	1.41	1.19	1.24	1.04	0.93	0.83	0.92	0.91	1.33	1.06	1.21	1.05
Min	0.62	0.94	1.02	0.88	0.93	0.80	0.70	0.59	0.60	0.65	0.97	0.84	0.96	0.83
β	**5.87**	**3.27**	2.32	**3.95**	**3.57**	**5.0**	**5.85**	**6.14**	**4.56**	**5.65**	2.85	**4.97**	**5.15**	5.02

Table 9
Effect of material types on $P_i/P_{ul\text{-}Exp}$ for different design approaches for GFRP-confined circular CFST short columns.

	P_{Lu2014} / $P_{ul\text{-}Exp}$ [12]	P_{Cao} / $P_{ul\text{-}Exp}$ [18]	P_{Ma2023}/ $P_{ul\text{-}Exp}$ [28]	$P_{Abdallah}$ /$P_{ul\text{-}Exp}$ [32]	P_{Lu2016}/ $P_{ul\text{-}Exp}$ [45]	$P_{Prop\text{-}Eq.36}$/ $P_{ul\text{-}Exp}$	$P_{Prop\text{-}Eq.38}$/ $P_{ul\text{-}Exp}$	$P_{Prop\text{-}Eq.41}$/ $P_{ul\text{-}Exp}$
$D/t \le 90(235/f_{ys})$								
(a) GFRP, normal strength steel and normal strength concrete (15 specimens)								
Avg	**0.95**	0.86	0.86	0.57	1.01	**1.00**	**1.07**	1.07
SD	0.18	0.183	0.178	0.078	0.173	0.134	0.145	0.143
Max	1.23	1.18	1.14	0.64	1.27	1.13	1.22	1.22
Min	0.69	0.64	0.61	0.43	0.75	0.81	0.87	0.87
β	2.83	**3.11**	**3.00**	**4.58**	2.68	**3.10**	**2.68**	2.69
(b) GFRP, normal strength steel and high strength concrete (23 specimens)								
Avg	**0.96**	0.88	**0.92**	0.66	1.03	**1.00**	**1.06**	1.06
SD	0.166	0.176	0.143	0.084	0.179	0.146	0.161	0.162
Max	1.28	1.25	1.20	0.85	1.37	1.23	1.31	1.31
Min	0.70	0.62	0.67	0.51	0.75	0.84	0.86	0.89
β	**3.07**	**3.19**	**3.46**	**5.12**	2.73	**3.16**	**2.75**	2.75
$D/t > 90(235/f_{ys})$								
(a) GFRP, normal strength steel and normal strength concrete (14 specimens)								
Avg	0.83	0.77	0.68	0.73	0.85	**0.97**	**1.01**	1.01
SD	0.101	0.091	0.093	0.080	0.107	0.065	0.064	0.065
Max	0.99	0.92	0.83	0.86	1.03	1.05	1.08	1.08
Min	0.68	0.64	0.56	0.61	0.70	0.87	0.91	0.91
β	**4.46**	**4.88**	**4.81**	**5.30**	**4.27**	**4.49**	**4.19**	4.16

obtain reliable results, calculating the lateral confining pressure has been separated into two formulae, as provided previously.

6.5. Biaxial stress state of the steel tube

For completion, this section explores a design resistance model which accounts for the bi-axial stresses that are experienced by the steel tubes in CFST columns. A reduction factor η_a is considered, as specified in EN 1994–1–1 [76] and as given in Eq. (39):

$$\eta_a = 0.25(3+2\lambda) \le 1.0 \tag{40}$$

where λ is the relative slenderness calculated as the square root of the plastic resistance to compression to the elastic critical normal force. By considering this reduction factor, and by using the same method defined in this paper, the expression for f_{rp} given in Eq. (40) is proposed, based on the regression analysis presented in Fig. 10:

$$f_{rp} = 1.332\left(\sqrt{f_{ys}f_{tf}}\right)\left(\frac{D}{\sqrt{t\times t_f}}\right)^{-0.841} \quad \text{For CFRP and GFRP, } R^2 = 0.632 \tag{41}$$

Based on the above, the design equation is proposed as:

$$P_{prop} = AptCommand019E;_a A_s f_{ys} + A_c\left(\gamma_c f_{cc} + k\left(1.332\left(\sqrt{f_{ys}f_{tf}}\right)\left(\frac{D}{\sqrt{t\times t_f}}\right)^{-0.841}\right)\right) \tag{42}$$

The results of this design method are presented in Tables 8 and 9 and the results are reasonable, but the reliability criteria for the GFRP-confined CFST columns is not satisfied. This highlights that this method can be used effectively with CFRP-confined CFST columns.

Table 10
Effect of material types on $P_i/P_{ul\text{-}Exp}$ for different design approaches for CFRP-confined square CFST short columns.

	P_{Ma2022} /$P_{ul\text{-}Exp}$ [14]	P_{Wei}/ $P_{ul\text{-}Exp}$ [38]	$P_{Zhang\ and\ Xiao}$/$P_{ul\text{-}Exp}$ [42]	P_{Cao} /$P_{ul\text{-}Exp}$ [18]	$P_{Wang\ and\ Shao}$/$P_{ul\text{-}Exp}$ [44]	$P_{Prop\text{-}Eq.36}$/ $P_{ul\text{-}Exp}$
$D/t \le 52((235/f_{ys})^{1/2})$						
(a) CFRP, normal strength steel and normal strength concrete (35 specimens)						
Avg	1.26	**0.93**	1.11	**0.95**	**1.02**	**0.98**
SD	0.148	0.110	0.170	0.118	0.120	0.102
Max	1.51	1.20	1.40	1.21	1.32	1.18
Min	1.06	0.77	0.77	0.79	0.89	0.84
β	1.67	**4.03**	2.23	**3.79**	**3.39**	**3.88**
(b) CFRP, normal strength steel and high strength concrete (17 specimens)						
Avg	1.43	1.10	1.11	1.11	1.15	**1.04**
SD	0.144	0.131	0.396	0.131	0.155	0.092
Max	1.62	1.27	1.98	1.28	1.37	1.17
Min	1.19	0.84	0.21	0.85	0.92	0.86
β	0.38	2.65	0.72	2.58	2.24	**3.46**
$D/t > 52((235/f_{ys})^{1/2})$						
(a) CFRP, normal strength steel and normal strength concrete (20 specimens)						
Avg	1.22	0.90	1.10	0.91	**0.95**	**0.97**
SD	0.158	0.139	0.259	0.139	0.176	0.109
Max	1.66	1.30	1.54	1.31	1.44	1.22
Min	1.06	0.73	0.45	0.76	0.79	0.83
β	1.97	**4.05**	1.44	**4.02**	**3.47**	**3.85**

7. Conclusions

This paper is concerned with the strength of FRP-confined concrete-filled steel tubular short columns. These are an increasingly popular structural solution owing to their high strength to weight properties, excellent durability and efficient use of the constituent materials. However, the paper highlights the lack of an accurate and reliable design model for these elements. The paper presents an extensive analysis of 324 experimental tests as described in the literature. These test programmes include samples with different geometric and material properties and the key variables examined include the cross-sectional shape, type of FRP, slenderness ratio of the steel tube, yield strength of the steel tube and concrete compressive strength. The test resistances of the columns are compared with the predictions obtained using ten different design models available in the literature for circular cross sections and four different approaches for square cross sections. It is shown that these are not always accurate or reliable for the full range of properties examined in the test database.

For this reason, the current work proposes a new confinement-based direct design resistance model for FRP-confined CFST short columns. This method is an advancement on earlier work, with the additional effect of the FRP wrapping in terms of confining pressure to the concrete core, included in the strength calculations. The proposed method is applicable for members with either a circular or square cross-section, and is validated based on available experimental results collected from the literature. Based on the study presented herein, the following conclusions are given:

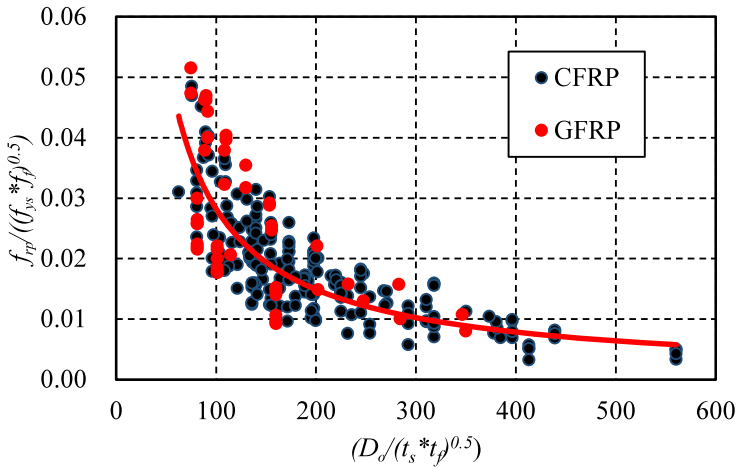

Fig. 9. Relationship between $\left(\frac{f_{rp}}{\sqrt{f_{ys}f_f}}\right)$ and $\frac{D}{\sqrt{t_s t_f}}$ ratios of FRP-confined circular CFST.

[1] The design models available in the literature provide moderate to highly conservative resistances for FRP-confined circular CFST short columns, with the exception of the models proposed by Wei, et al. [7] and Park, et al. [9] which provide moderate to unconservative predictions.

[2] All of the design models available in the literature provide moderate to unconservative resistances for FRP-confined square CFST short columns. Moreover, the methods presented by Wei, et al. [38], Cao, et al. [18] and Wang and Shao [44] result in acceptable reliability indices β which are greater than 3.0.

[3] It is shown that the accuracy and reliability of the design methods available in the literature is dependant on the slenderness ratio of the structural element.

[4] The confinement-based direct design resistance model which is proposed herein, and includes a procedure for calculating the lateral confining pressure on the concrete as a result of the FRP confinement (f_{rp}) is shown to provide the most accurate and reliable capacity predictions of all the methods examined, for the extensive experimental database. It is also shown to be accurate for a range of material and geometric properties. It should be noted that the confinement coefficient (triaxial factor) is to be taken as 2.86 [9,72] for the correct use of this confinement-based direct design resistance model.

[5] Despite considering a unified equation for GFRP- and CFRP-confined CFST columns, the reduction in stress of the steel tubes provided good results in general but the reliability analyses of GFRP-confined CFST columns have not shown acceptable results.

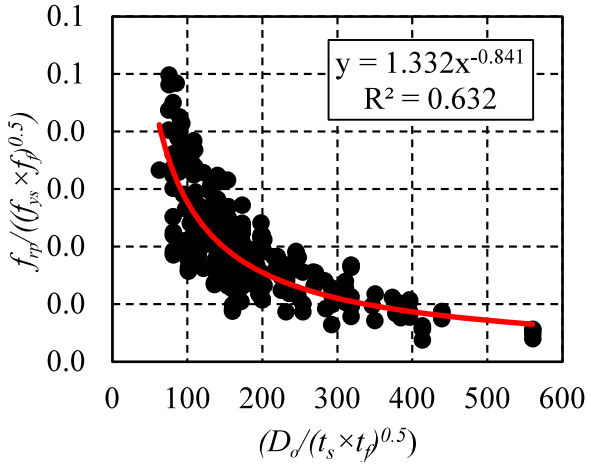

Fig. 10. Relationship between $\left(\frac{f_{rp}}{\sqrt{f_{ys}f_f}}\right)$ and $\frac{D}{\sqrt{t_s t_f}}$ ratios of FRP-confined CFST.

Finally, it is noteworthy that there is a dearth of data in the literature for FRP-confined circular or square CFST short columns with HSC or UHSC and a relatively high slenderness ratio. Therefore, this is recommended as a subject for future research. Additionally, it is recommended that attention should be given to the analysis of the design parameters, as employed in the large database of results collated herein. Moreover, a design model based on the strain limit of the CFRP material could be derived in future.

CRediT authorship contribution statement

M.F. Hassanein: Investigation, Writing – original draft, Writing – review & editing. **Asmaa Y. Hamed:** Investigation. **K.A. Cashell:** Writing – original draft, Writing – review & editing. **Yong-Bo Shao:** Investigation.

Declaration of Competing Interest

The authors declare that they have no known competing financial interests or personal relationships that could have appeared to influence the work reported in this paper.

Data availability

Data will be made available on request.

References

[1] G.J. Teng, F.J. Chen, T.S. Smith and L. Lam, "FRP Strengthened RC Structures," John Wiley & Sons, Ltd..
[2] G.J. Teng, L. Lam, Behavior and modeling of fiber reinforced polymer-confined concrete, J. Struct. Eng., ASCE 130 (11) (2004), 1713-173.
[3] Y. Xiao, H.W. He, K.K. Choi, Confined concrete filled tubular columns, J. Struct. Eng., ASCE 131 (3) (2005) 488–497.
[4] D. Lam, H.A. Clark, Strengthening steel sections using carbon fibre reinforced polymers laminates, in: Proceedings of the International Conference on Advances in Structures, Sydney, Australia, 2003, pp. 1369–1374. June.
[5] K. ChoI, Y. Xiao, Analytical model of circular CFRP confined concrete-filled steel tubular columns under axial compression, J. Compos. Constr 14 (2010) 125–133.
[6] L.N. Ding, X. Liu, X. Wang, H.J. Huang, Z.S. Wu, Mechanical properties of pultruded basalt fiber-reinforced polymer tube under axial tension and compression, Constr. Build. Mater 178 (2018) 629–637.
[7] Y. Wei, G. Wu, G. Li, Performance of circular concrete-filled fiber-reinforced polymer-steel composite tube columns under axial compression, J. Reinforced Plastics and Compos. 33 (20) (2014) 1911–1928.

[8] L. Liu, Y. Lu, Axial bearing capacity of short FRP confined concrete-filled steel tubular columns, J. Wuhan University of Technol.-Mater. Sci. Ed 25 (3) (June 2010) 455–485.
[9] J.W. Park, Y.K. Hong, G.S. Hong, J.H. Kim, S.M. Ch, Design formulas of concrete filled circular steel tubes reinforced by carbon fiber reinforced plastic sheets, Procedia Eng. 14 (2011) 2916–2922.
[10] Z. Tao, L.H. Han, J.P. Zhuang, Axial loading behavior of CFRP strengthened concrete-filled steel tubular stub columns, Adv. Struct. Eng 10 (2007) 37–46.
[11] J.P. Liu, T.X. Xu, Y.H. Wang, Y. Guo, Axial behaviour of circular steel tubed concrete stub columns confined by CFRP materials, Constr. Build. Mater 168 (2018) 221–231.
[12] Y.Y. Lu, N. Li, S. Li, Behavior of FRP-confined concrete-filled steel tube columns, Polym. Bull. 6 (2014) 1333–1349.
[13] Y. Che, Q.L. Wang, Y.B. Shao, Compressive performances of the concrete filled circular CFRP-steel Tube (C-CFRP-CFST), Adv. Steel Constr. 8 (2012) 331–358.
[14] L. Ma, C. Zhou, D. Lee, J. Zhang, Prediction of axial compressive capacity of CFRP-confined concrete-filled steel tubular short columns based on XGBoost algorithm, Eng. Struct. 260 (2022), 114239.
[15] F.X. Ding, D.R. Lu, Y. Bai, Y.Z. Gong, Z.W. Yu, M. Ni, Behaviour of CFRP confined concrete-filled circular steel tube stub columns under axial loading, Thin-Walled Struct. 125 (2018) 107–118.
[16] J. Deng, Y.F. Zheng, W. Yi, T.H. Liu, H. Li, Study on axial compressive capacity of FRP confined concrete-filled steel tubes and its comparisons with other composite structural systems, Int. J. Ploym. Sci. (2017) 1–7, https://doi.org/10.1155/2017/6272754.
[17] J.L. Zhao, C.H. Xu, L.Z. Sun, D.Y. Wu, Behaviour of FRP-confined compound concrete–filled circular thin steel tubes under axial compression, Adv. Struct. Eng. 23 (9) (2020) 1772–1784, https://doi.org/10.1177/1369433219900941.
[18] S. Cao, C. Wu, W. Wang, Behavior of FRP confined UHPFRC-filled steel tube columns under axial compressive loading, J. Build. Eng. 32 (2020), 101511.
[19] Q.H. Shen, J.H. Wang, J.X. Wang, Z.D. Ding, Axial compressive performance of circular CFST columns partially wrapped by carbon FRP, J. Constr. Steel Res. 155 (2019) 90–106, https://doi.org/10.1016/j.jcsr.2018.12.017.
[20] J. Liu, T. Xu, Y. Guo, X. Wang, Y.F. Chen, Behavior of circular CFRP-steel composite tubed high-strength concrete columns under axial compression, Compos. Struct. 211 (2019) 596–609.
[21] J. Zhang, L. Ma, C. Zhou, D. Lee, F.C. Filippou, Experimental study of axial compression behavior of circular concrete-filled steel tubes after being loaded at an early age, Construct. Build. Mater. 300 (2021), 124020.
[22] J.J. Zeng, Y.W. Zheng, F. Liu, Y.C. Guo, C. Hou, Behavior of FRP ring-confined CFST columns under axial compression, Compos. Struct. 257 (2021), 113166, https://doi.org/10.1016/j.compstruct.2020.113166.
[23] C.N. Xiong, Y.B. Shao, L.W. Tong, K.S. Dai, Y.X. Luo, Static strength of CFRP-strengthened preloaded circular concrete-filled steel tube stub columns, Part I: experimental test, Thin-walled Struct. 184 (2023), 110546.
[24] S. Zhang, K. Miao, Y. Wei, X. Xu, B. Luo, W. Shi, Experimental and theoretical study of concretefilled steel tube columns strengthened by FRP/Steel strips under axial compression, Int. J.Concrete Struct. Mater. 17 (2023).
[25] G.S. Sun, Y.H. Zhao, W. Gu, Stability of concrete filled CFRP steel tube under axial compression, in: Tubular structure XII, London, Taylor & Francis Group., 2009.
[26] N.A. Alwash, H.I. Al-Salih, Experimental investigation on behavior of SCC filled steel tubular stub columns strengthened with CFRP, Constr. Eng. 1 (2) (2013) 37–51.
[27] Q.L. Wang, J.Y. Wang, Y.D. Zhang, D. Yong, Mechanical property analysis on axially compressed concrete filled circular CFRP-steel tube stub columns, Eng. Mech. 23 (8) (Aug. 2006), 1000-4750(2006)08-0102-04.
[28] Y. Ma, K. Ma, X. Han, T. Yao, Experimental investigation of FRP-confined HSC-filled steel tube stub columns under axial compression, Eng. Struct. 280 (2023), 115670.
[29] W. Gu, C.W. Guan, Y.H. Zhao, H. Cao, Experimental study on concentrically-compressed circular concrete filled CFRP-steel composite tubular short columns, J. Shenyang Arch. & Civil Eng. Inst 20 (2) (2004) 118–120.
[30] L. Na, L. Yiyan, L. Shan, L. Lan, Slenderness effects on concrete-filled steel tube columns confined with CFRP, J. Constructional Steel Res. 143 (2018) 110–118, https://doi.org/10.1016/j.jcsr.2017.12.014.
[31] T. Yu, Y.M. Hub, J.G. Teng, FRP-confined circular concrete-filled steel tubular columns under cyclic axial compression, J. Constructional Steel Res. 94 (2014) 33–48, https://doi.org/10.1016/j.jcsr.2013.11.003.
[32] S. Abdalla, F. Abed, M. AlHamaydeh, Behavior of CFSTs and CCFSTs under quasi-static axial compression, J. Constructional Steel Res. 90 (2013) 235–244, https://doi.org/10.1016/j.jcsr.2013.08.007.
[33] S. Abdalla, Master's thesis, American University of Sharjah, UAE, 2012.
[34] Y.M. Hu, T. Yu, J.G. Teng, FRP-confined circular concrete-filled thin steel tubes under axial compression, J. Compos. Constr 15 (2011) 850–860.
[35] J.G. Teng, Y.M. Hu, Theoretical model for FRP-confined circular concrete-filled steel tubes under axial compression, in: Third international conference on FRP Composites in Civil Engineering (CICE 2006), Miami, Florida, USA, 2006.
[36] J.W. Park, S.H. Chung, The experiment and design formula of rectangular CFT columns reinforced by carbon fiber sheets, J. Korea Academia-Ind. Cooperation Soc. 11 (10) (2010) 4024–4030, https://doi.org/10.5762/KAIS.2010.11.10.4024.
[37] J.W. Park, Y.K. Hong, S.M. Choi, Behaviors of concrete filled square steel tubes confined by carbon fiber sheets (CFS) under compression and cyclic loads, Steel Compos. Struct. 10 (2) (2010) 187–205, https://doi.org/10.12989/scs.2010.10.2.187.
[38] Y. Wei, Y.R. Zhang, J.L. Chai, G. Wu, Z.Q. Dong, Experimental investigation of rectangular concrete-filled fiber reinforced polymer (FRP)-steel composite tube columns for various corner radii, Compos. Struct. 244 (2020), 112311, https://doi.org/10.1016/j.compstru.
[39] Q.L. Wang, Z. Zhao, Y.B. Shao, Q.L. Li, Static behavior of axially compressed square concrete filled CFRP-steel tubular (S-CF-CFRP-ST) columns with moderate slenderness, Thin-Walled Struct. 110 (2017) 106–122.
[40] J.F. Liang, W.J. Zou, Z.L. Wang, D.W. Liu, Compressive behavior of CFRP confined partially encased concrete columns under axial loading, Compos. Struct. 229 (2019), 111479, https://doi.org/10.1016/j.compstruct.2019.111479.
[41] G.C. Li, L. Ma, J.L. Yang, Bearing capacity of short columns of high-strength concrete filled square steel tubular with inner CFRP circular tubular under axially compressive load, J. Shenyang Jianzhu University 24 (1) (2008) 62–66.
[42] Y.T. Zhang, Y. Xiao, Study on behaviors of FRP confined stub concrete filled square steel tubes under axial load, J. Hunan Univ. (Nat Sci) 46 (11) (2019) 50–60, https://doi.org/10.16339/j.cnki.hdxbzkb.2019.11.006, in Chinese.
[43] C.X. Dong, A.K. Kwan, J.C. Ho, Effects of external confinement on structural performance of concrete-filled steel tubes, J. Const. Steel Res. 132 (2017) 72–82.
[44] Q. Wang, Y.B. Shao, Compressive performances of concrete filled Square CFRP-Steel Tubes (S-CFRP-CFST), Steel and Compos. Structures 16 (5) (2014) 455–480, https://doi.org/10.12989/scs.2014.16.5.455.
[45] Y.Y. Lu, S. Li, S. Li, N. Li, Study on property of concentrically compressed concrete filled circular FRP-steel tube stub columns, J. China Railway Soc. 38 (4) (2016) 105–111, https://doi.org/10.3969/j.issn.1001-8360.2016.04.015, in Chinese.
[46] H.Y. Tang, J.L. Chen, L.Y. Fan, X.J. Sun, C.M. Peng, Experimental investigation of FRP confined concrete-filled stainless steel tube stub columns under axial compression, Thin-Walled Struct. 146 (2020), 106483, https://doi.org/10.1016/j.tws.2019.106483.
[47] M. Soman, C.R. Chandrase kharannair, Axial behaviour of glass fibre reinforced polymer- confined reinforced concrete short columns, Struct. Eng. Int. 28 (1) (2018) 44–50, https://doi.org/10.1080/10168664.2018.1431422.
[48] Y. Zhang, Y. Wei, J. Bai, Y. Zhang, Stress-strain model of an FRP-confined concrete filled steel tube under axial compression, Thin-Walled Struct. 142 (2019) 149–159.
[49] E.M. Güneyisia, A.I. Nour, Axial compression capacity of circular CFST columns transversely strengthened by FRP, Eng. Struct. 191 (2019) 417–431.
[50] J.G. Teng, Y.M. Hu, T. Yu, Stress-strain model for concrete in FRP-confined steel tubular columns, Eng. Struct. 49 (2013) 156–167.
[51] G.G. Prabhu, M.C. Sundarraja, Behaviour of concrete filled steel tubular (CFST) short columns externally reinforced using CFRP strips composite, Constr Build Mater 47 (10) (2013) 1362–1371, https://doi.org/10.1016/j.conbuildmat.2013.06.038.
[52] M.C. Sundarraja, G.G. Prabhu, Experimental study on CFST members strengthened by CFRP composites under compression, J. Constr. Steel Res. 72 (2012) 75–83, https://doi.org/10.1016/j.jcsr.2011.10.014.
[53] A. Parvin, A.S. Jamwal, Effects of wrap thickness and ply configuration on composite confined concrete cylinders, Compos. Struct. 67 (2005) 437–442.
[54] T T. Jiang, J.G. Teng, Analysis-oriented stress–strain models for FRP-confined concrete, Eng. Struct. 29 (11) (2007) 2968–2986.
[55] Eurocode 2, "Design of concrete structures. Part 1-1," General rules and rules for, buildings, 2004," 2004.
[56] S.A. Mirza, E.A. Lacroix, Comparative strength analyses of concrete-encased steel composite columns, J. Struct. Eng., ASCE 130 (12) (2004) 1941–1953.
[57] N.E. Shanmugam, B. Lakshmi, State of the art report on steel-concrete composite columns, J. Constr. Steel Res 57 (2001) 1041–1080.
[58] L.H. Han, L. Wei, R. Bjorhovde, Developments and advanced applications of concrete-filled steel tubular (CFST) structures: members, J. Constr. Steel Res 100 (2014) 211–228.
[59] M.K. Ravindra, T.V. Galambos, Load and resistance factor design for steel, J. Struct. Division 104 (1978) 1337–1353.
[60] Z. Lai, A.H. Verma, High-strength rectangular CFT members: database, modeling, and design of short columns, J. Struct. Eng. 144 (4) (2018) 18–36.
[61] S. Thai, H.T. Thai, B. Uy, T. Ngo, Concrete-filled steel tubular columns: test database, design and calibration, J. Construct. Steel Res. 157 (2019) 161–181.
[62] M.F. Hassanein, N. Silvestre, New confining stress-based design for rubberised concrete-filled single/double-skin steel tubular short columns, J. Construct. Steel Res. 197 (2022), 107435.
[63] R.M. Bartlett, R.M. Dexter, R.J. Graeser, J.J. Jelinek, B.J. Schmidt, Galambos, Updating standard shape material properties database for design and reliability, Eng. J. 40 (1) (2003) 2–14.
[64] J. Chen, PHD, The Hong Kong Polytechnic University, 2020.
[65] ASCE, Minimum design loads for buildings and other structures, in: ASCE/SEI 7-10, Reston, Virginia, American Society of Civil Engineers, 2010.
[66] M.F. Hassanein, A.Y. Hamed, Y.B. Shao, N. Silvest, Confinement-based direct design of circular steel tube confined concrete (STCC) short columns, J. Constructional Steel Res. 204 (2023), 107871.
[67] W.F. Huang, Y.B. Shao, M.F. Hassanein, Behaviour and confinement-based direct design of concrete-filled cold-formed stiffened steel tubular short columns, J. Construct. Steel Res. 202 (2023), 107773.
[68] M.F. Hassanein, N. Silvestre, X.F. Yan, Confinement-based direct design of circular concrete-filled double-skin normal and high strength steel short columns, Thin-Walled Struct. 183 (2023), 110446.
[69] Y. Xu, Y.B. Shao, M.F. Hassanein, N. Silvestre, Innovative compressive design resistance and behaviour of concrete-filled short columns with stiffened square steel sections, J. Constructional Steel Res. 198 (2022), 107510.
[70] Q.Q. Liang, Performance-based analysis of concrete-filled steel tubular beam–columns, part i: theory and algorithms, J. Construct. Steel Res. 65 (2) (2009) 363–373, https://doi.org/10.1016/j.jcsr.2008.03.007.

[71] E. Richart, R.L. Brandzaeg, R.L. Brown, Failure of plain and spirally reinforced concrete in compression. Bulletin 190, University of Illinois Engineering Experimental Station, Champaign, 1929.
[72] K. Cederwall, Some ideas and studies concerning the ultimate capacity of composite steel and concrete elements, Nordic Concrete J. 5 (1988) 8–14. http://worldcat.org/issn/00291307.
[73] L. Lam, G. Teng, Strength models for fiber-reinforced plastic-confined concrete, J. Struct. Eng., ASCE 128 (5) (2002) 612–623.
[74] S. Matthys, H. Toutanji, K. Audenaert, L. Taerwe, Axial load behavior of largescale columns confined with FRP composites, ACI Struct. J. 102 (2) (2005) 258–267.
[75] M. Johansson, Ph.D. thesis, Chalmers University of Technology, Goteborg, Sweden, 2002.
[76] Eurocode 4, Design of Composite Steel and Concrete Structures Part 1–1: General Rules and Rules for Buildings, CEN, Brussels, Belgium, 2004.
[77] Y. Du, Y. Zhang, Z. Chen, J.B. Yan, Z. Zheng, Axial compressive performance of CFRP confined rectangular CFST columns using high-strength materials with moderate slenderness, Construction and Build. Mater. 299 (2021), 123912.
[78] B.W. Schafer, Review: the direct strength method of cold-formed steel member design, J. Construct. Steel Res. 64 (2008) 766–778.
[79] L. Gardner, X. Yun, F. Walport, The continuous strength method – review and outlook, Eng. Struct. 114924 (2023) 275.
[80] M. Zarringol, V.I. Patel, Q.Q. Linag, Artificial neural network model for strength predictions of CFST columns strengthened with CFRP, Eng. Struct. 281 (2023), 115784.